Self-Assembling Porphyrin [2]-Catenanes

Maxwell J. Gunter,*,† David C. R. Hockless,‡ Martin R. Johnston,† Brian W. Skelton,‡ and Allan H. White‡

Contribution from the Department of Chemistry, The University of New England, Armidale, NSW 2351, Australia, and the Department of Chemistry, University of Western Australia, Nedlands, WA 6009, Australia

*Received December 9, 1993. Revised Manuscript Received March 14, 1994**

Abstract: Using the concepts of self-assembly developed for the construction of topologically complex molecules such as [2]-catenanes and rotaxanes, the syntheses of several prophyrin–catenanes are described. The successful insertion of the porphyrin subunit into [2]-catenanes has resulted from the adaptation of previously devised template-directed syntheses based primarily on π–π interactions and C–H···O and C–H···π hydrogen bonding. Several hydroquinol-containing ether chains were successfully synthesized and subsequently strapped across a porphyrin ring; the X-ray crystal structures of two such molecules which vary in the length of the ether chain are reported. These strapped porphyrins were found to complex paraquat with a parallel orientation of the hydroquinol, paraquat, and porphyrin rings. The complexation of paraquat (K_a = 1955 and 1640 M^{-1}, $\Delta G°$ = –4.5 and –4.4 kcal mol^{-1} for **9** and **11**, respectively) by these strapped porphyrins led to their subsequent inclusion, using template-directed self-assembly, into structures which represent the first examples of porphyrin-containing [2]-catenanes. The catenanes were subsequently characterized by FAB-MS and thoroughly examined using dynamic ^1H NMR. In the case of the hydroquinol-containing catenanes, a dynamic process was observed in solution in which the bipyridinium subunits of the tetracation were exchanged between "inside" and "outside" environments (rotation around the hydroquinol ring axis). The diethylene glycol containing catenanes **14** and **15** were observed to maintain an orientation of the tetracation in which the bipyridinium subunits are parallel to the porphyrin ring. The length of the ether strap in these catenanes influenced the rotation rates of the tetracation macrocycles (50 and 80 times per second for **14** and **15** and 2500 and 1500 times per second for **16** and **17**, respectively) at ambient temperature. However, in all the catenanes, the overall orientation of the tetracation, with bipyridinium and porphyrin rings coparallel, is retained in solution. As an extension of the original concepts, an analogous strapped porphyrin containing a naphthoquinol moiety was synthesized and found to complex paraquat with K_a = 21 000 M^{-1} and $\Delta G°$ = –5.9 kcal mol^{-1}. The general applicability of the template-directed synthetic procedure developed for porphyrin catenane synthesis was illustrated by the successful isolation of the naphthalene-containing porphyrin [2]-catenane **23** in 45% yield. Tetracation exchange processes similar to those for the hydroquinol catenanes were observed, along with an additional process which was found to be the decomplexation/complexation of the naphthalene ring in what is termed an "out, turn around, and in again" process similar to that occurring in nonporphyrinic naphthalene [2]-catenanes.

Introduction

Topologically complex molecules such as catenanes, rotaxanes, and knots have until recently been regarded as mere academic curiosities,[1,2] but their potential as components of molecular-scale devices is now being realized. The synthetic strategies for the construction of such molecules have until recently been dominated by methodologies such as statistical threading and the Möbius strip approach, and these have recently been reviewed.[3] However, the application of the concepts of supramolecular chemistry has revolutionized the ability of the synthetic chemist to construct such complicated structures[3,4] and especially so in the application of the processes of *self-assembly*,[5–7] utilizing a variety of noncovalent interactions between constituent parts. For example, the complexing ability of various cyclodextrins has been employed to enhance the threading of various alkyl-[8,9] and aromatic-based[10] chains, leading to the formation of several rotaxanes, polyrotaxanes,[11,12] and catenane structures.[13] Sauvage and others have employed metal ion templating to construct a vast array of catenates and catenands,[3,14] rotaxanes,[15] and knots.[16,17] The use of π–π electron interactions in combination with hydrogen bonding,[4,18] as well as electrostatic interactions, has been useful in self-assembly of an impressive body of catenanes,[2,19–24]

† University of New England.
‡ University of Western Australia.
* Abstract published in *Advance ACS Abstracts,* May 1, 1994.

(1) Schill, G. *Catenanes, Roxanes, and Knots*; Academic Press: New York, 1971.
(2) Anelli, P. L.; Ashton, P. R.; Ballardini, R.; Balzani, V.; Delgado, M.; Gandolfi, M. T.; Goodnow, T. T.; Kaifer, A. E.; Philp, D.; Pietraszkiewicz, M.; Prodi, L.; Reddington, M. V.; Slawin, A. M. Z.; Spencer, N.; Stoddart, J. F.; Vicent, C.; Williams, D. J. *J. Am. Chem. Soc.* **1992**, *114*, 193–218.
(3) Dietrich-Buchecker, C. O.; Sauvage, J.-P. *Chem. Rev.* **1987**, *87*, 795–810.
(4) Hunter, C. A. *J. Am. Chem. Soc.* **1992**, *114*, 5303–5311.
(5) Stoddart, J. F. *Chem. Brit.* **1991**, 714–718.
(6) Stoddart, J. F. In *Host-guest Molecular Interactions: From Chemistry to Biology (Ciba Foundation Symposium)*; John Wiley and Sons: Chichester, U.K., 1991; pp 5–22.
(7) Whitesides, G. M.; Mathias, J. P.; Seto, C. T. *Science* **1991**, *254*, 1312–1319.
(8) Isnin, R.; Kaifer, A. E. *J. Am. Chem. Soc.* **1991**, *113*, 8188–8190.
(9) Wylie, R. S.; Macartney, D. H. *J. Am. Chem. Soc.* **1992**, *114*, 3136–3138.
(10) Wenz, G.; von der Bey, E.; Schmidt, L. *Angew. Chem., Int. Ed. Engl.* **1992**, *31*, 783–785.
(11) Wenz, G.; Keller, B. *Angew. Chem., Int. Ed. Engl.* **1992**, *31*, 197–199.
(12) Stoddart, J. F. *Angew. Chem., Int. Ed. Engl.* **1992**, *31*, 846.
(13) Armspach, D.; Ashton, P. R.; Moore, C. P.; Spencer, N.; Stoddart, J. F.; Wear, T. J.; Williams, D. J. *Angew. Chem., Int. Ed. Engl.* **1993**, *32*, 854.
(14) Albrecht-Gary, A.-M.; Dietrich-Buchecher, C. O.; Saad, Z.; Sauvage, J.-P. *J. Chem. Soc., Chem. Commun.* **1992**, 280–282.
(15) Chambron, J.-C.; Heitz, V.; Sauvage, J.-P. *J. Chem. Soc., Chem. Commun.* **1992**, 1131–1133.
(16) Dietrich-Buchecker, C. O.; Nierengarten, J.-F.; Sauvage, J.-P. *Tetrahedron Lett.* **1992**, *33*, 3625–3628.
(17) Walba, D. M.; Zheng, Q. Y.; Schilling, K. *J. Am. Chem. Soc.* **1992**, *114*, 6259–6260.
(18) Vögtle, F.; Meier, S.; Hoss, R. *Angew. Chem., Int. Ed. Engl.* **1992**, *31*, 1619.
(19) Ashton, P. R.; Goodnow, T. T.; Kaifer, A. E.; Reddington, M. V.; Slawin, A. M. Z.; Spencer, N.; Stoddart, J. F.; Vicent, C.; Williams, D. J. *Angew. Chem., Int. Ed. Engl.* **1989**, *28*, 1396–1399.

0002-7863/94/1516-4810$04.50/0

rotaxanes[2,25-28](including "*molecular shuttles*"[26,29,30] and a "*molecular train set*"[5,31]), and pseudo-rotaxanes.[32-34] While all of the above strategies have particular applicabilities, the subsequent discussion will center on $\pi-\pi$ electron and electrostatic interactions, as developed by Stoddart, in the synthesis of [2]-catenanes.

The science of *nanotechnology*, *molecular cybernetics*,[6] or *molecular informatics*[35] is based on the construction of molecular machines[36] from carefully designed components, using self-assembly strategies[7] and template-directed syntheses, to create assemblies which have potential for use in a variety of possible applications, such as the storage and transfer of information at a molecular level.[2,35,37] More recent activity in this area has been directed toward the incorporation of components with functionalities that may be addressed through chemical, photochemical, or electrochemical means. In particular, attention has been focused on the porphyrin macrocycle whose characteristics in these areas have been thoroughly documented. The inclusion of porphyrins in rotaxanes has been reported by both Stoddart[26] and Sauvage[15] and in catenanes by us.[23] Incorporation of porphyrin subunits within these structures allows an expansion into the vast body of chemistry that characterizes these macrocycles in such areas as electrochemistry, photochemistry, and metal coordination. The use of porphyrins in self-assembling molecular architectures is a logical next step, allowing multicomponent systems to be constructed which might exhibit novel electronic and photochemical properties.[15]

The template-directed synthetic strategy developed for porphyrin inclusion within catenanes is an extension of the concepts originally developed by Stoddart for catenane synthesis,[38-40] which have been thoroughly refined and employed to produce an impressive array of supramolecular assemblies. The fundamental component for catenane assembly is a bis-hydroquinol- or naphthoquinol-containing crown ether of appropriate size (such as bis(*p*-phenylene)-34-crown-10, BPP34C10 (**2**), or the corresponding naphthoquinol analogue 1,5-dinaphtho-38-crown-10,

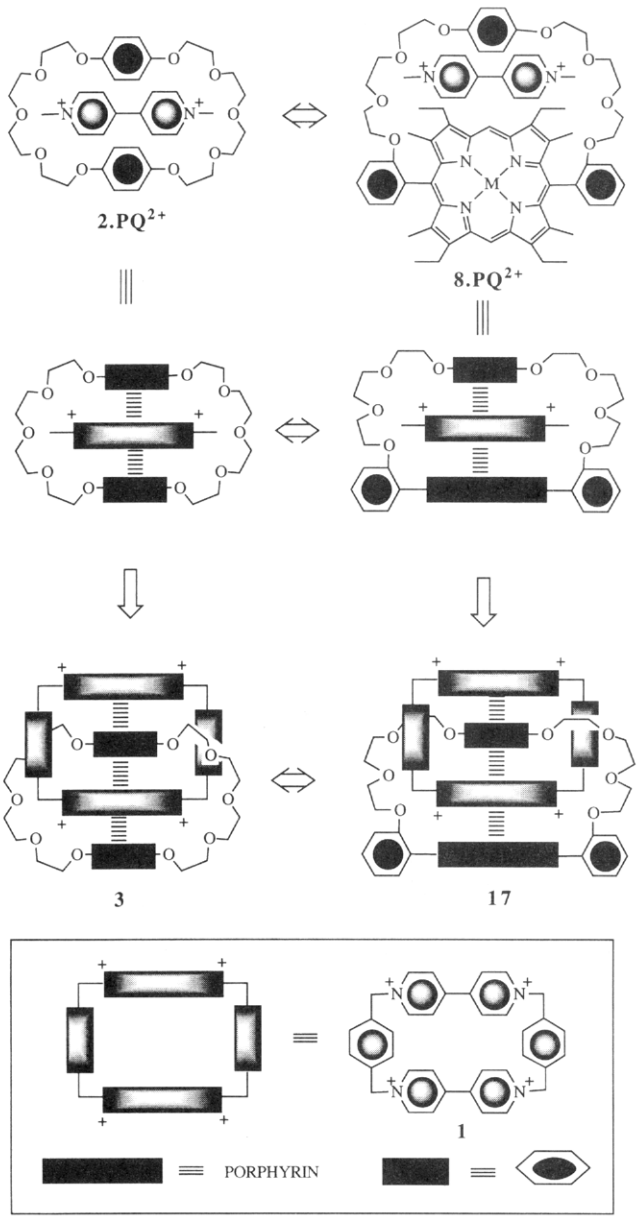

Figure 1. Schematic representation of the evolution of the design strategy developed by Stoddart for the synthesis of the [2]-catenane **3**[19] and its subsequent extension by us to facilitate the inclusion of a porphyrin macrocycle into [2]-catenane **17**. The black and white cartoons follow those adopted in color by Stoddart;[19] the solid rectanges represent π-electron-rich systems, and shaded boxes are used for π-electron-deficient systems. Additionally, the larger solid rectangle has been included in this case to represent the porphyrin moiety.

1,5DN38C10) which can complex the bipyridinium dication paraquat (1,1′-dimethyl-4,4′-bipyridinium). Template-directed self-assembly of the appropriate components results in efficient synthesis of catenanes, with the tetracationic macrocycle **1** interlinked with the cyclic crown ether (Figure 1). The self-assembly process relies on C–H···O and C–H···π hydrogen bonding and $\pi-\pi$ interactions between the initially formed bipyridinium cations and the hydroquinol- or naphthoquinol-containing crown ether. Since $\pi-\pi$ electron interactions are of fundamental importance in these systems, for both paraquat complexation and subsequent catenane formation, we reasoned that the replacement of one of the electron-rich hydroquinol or naphthoquinol units of the crown ether by a porphyrin ring, with its large π-electron-rich nucleus, should enhance paraquat complexation as well as encourage catenane formation in the usual manner. This strategy is outlined in Figure 1. A porphyrin suitable for paraquat complexation in a manner analogous to

(20) Ashton, P. R.; Brown, C. L.; Chrystal, E. J. T.; Goodnow, T. T.; Kaifer, A. E.; Parry, K. P.; Philp, D.; Slawin, A. M. Z.; Spencer, N.; Stoddart, J. F.; Williams, D. J. *J. Chem. Soc., Chem. Commun.* **1991**, 634–639.
(21) Ashton, P. R.; Brown, C. L.; Chrystal, E. J. T.; Goodnow, T. T.; Kaifer, A. E.; Parry, K. P.; Slawin, A. M. Z.; Spencer, N.; Stoddart, J. F.; Williams, D. J. *Angew. Chem., Int. Ed. Engl.* **1991**, *30*, 1039–1042.
(22) Brown, C. L.; Philp, D.; Stoddart, J. F. *Synlett* **1991**, 459–464.
(23) Gunter, M. J.; Johnston, M. R. *J. Chem. Soc., Chem. Commun.* **1992**, 1163–1165.
(24) Ashton, P. R.; Reder, A. S.; Spencer, N.; Stoddart, J. F. *J. Am. Chem. Soc.* **1993**, *115*, 5286–5287.
(25) Ashton, P. R.; Grognuz, M.; Slawin, A. M. Z.; Stoddart, J. F.; Williams, D. J. *Tetrahedron Lett.* **1991**, *32*, 6235–6238.
(26) Ashton, P. R.; Johnston, M. R.; Stoddart, J. F.; Tolley, M. S.; Wheeler, J. W. *J. Chem. Soc., Chem. Commun.* **1992**, 1128–1131.
(27) Ashton, P. R.; Bělohradsky, M.; Philp, D.; Stoddart, J. F. *J. Chem. Soc., Chem. Commun.* **1993**, 1269–1274.
(28) Ashton, P. R.; Bělohradsky, M.; Philp, D.; Spencer, N.; Stoddart, J. F. *J. Chem. Soc., Chem. Commun.* **1993**, 1274–1277.
(29) Anelli, P. L.; Spencer, N.; Stoddart, J. F. *J. Am. Chem. Soc.* **1991**, *113*, 5131–5133.
(30) Ashton, P. R.; Philp, D.; Spencer, N.; Stoddart, J. F. *J. Chem. Soc., Chem. Commun.* **1992**, 1124–1128.
(31) Ashton, P. R.; Brown, C. L.; Chrystal, E. J. T.; Parry, K. P.; Pietraszkiewicz, M.; Spencer, N.; Stoddart, J. F. *Angew. Chem., Int. Ed. Engl.* **1991**, *30*, 1042–1045.
(32) Ashton, P. R.; Philp, D.; Spencer, N.; Stoddart, J. F. *J. Chem. Soc., Chem. Commun.* **1991**, 1677–1679.
(33) Ashton, P. R.; Philp, D.; Reddington, M. V.; Slawin, A. M. Z.; Spencer, N.; Stoddart, J. F.; Williams, D. J. *J. Chem. Soc., Chem. Commun.* **1991**, 1680–1683.
(34) Anelli, P. L.; Ashton, P. R.; Spencer, N.; Slawin, A. M. Z.; Stoddart, J. F.; Williams, D. J. *Angew. Chem., Int. Ed. Engl.* **1991**, *30*, 1036–1039.
(35) Lehn, J.-M. *Angew. Chem., Int. Ed. Engl.* **1990**, *29*, 1304–1319.
(36) Stoddart, J. F. *Chem. Aust.* **1992**, 576–577.
(37) Philp, D.; Stoddart, J. F. *Synlett* **1991**, 445–458.
(38) Allwood, B. L.; Spencer, N.; Shahriari-Zavareh, H.; Stoddart, J. F.; Williams, D. J. *J. Chem. Soc., Chem. Commun.* **1987**, 1064–1066.
(39) Odell, B.; Reddington, M. V.; Slawin, A. M. Z.; Spencer, N.; Stoddart, J. F.; Williams, D. J. *Angew. Chem., Int. Ed. Engl.* **1988**, *27*, 1547–1550.
(40) Ortholand, J.-Y.; Slawin, A. M. Z.; Spencer, N.; Stoddart, J. F.; Williams, D. J. *Angew. Chem., Int. Ed. Engl.* **1989**, *28*, 1394–1395.

Table 1. Selected Resonances for the Strapped Porphyrins and Chemical Shift Changes from Their Equimolar Solutions with Paraquat Dication in Dimethylformamide-d_7[a]

	H1	H4	H16	H17	H18	H19	H20	H21	HQ	α,α′	β,β′	+N-Me
PQ^{2+}										9.52	8.95	4.72
8[a]	10.27	4.05	4.34	3.47	2.98	1.75			3.83			
9[b]	10.19	4.05	4.42	3.40	2.92	2.06			3.84			
9/PQ^{2+} 1:1[b]	9.97	4.02[c] 3.92[c]	4.52	3.57	3.18	2.60			4.69	8.98	7.99	4.42
Δδ[d]	(–0.22)	(+0.03) (–0.13)	(+0.10)	(+0.17)	(+0.26)	(+0.54)			(+0.85)	(–0.54)	(–0.96)	(–0.30)
10[a]	10.22	4.04	4.20	3.35	2.77	2.57	2.48	2.48	5.48			
11[b]	10.16	4.04	4.34	3.47	2.99	2.92	2.97	2.97	5.76			
11/PQ^{2+} (1:1)[b,e]	10.10	4.01[c] 3.91[c]	4.42	3.55	3.12	3.02	3.05	3.05	5.74	8.98	7.99	4.47
Δδ[d]	(–0.06)	(+0.03) (–0.13)	(+0.08)	(+0.08)	(+0.13)	(+0.10)	(+0.08)	(+0.08)	(+0.02)	(–0.54)	(–0.96)	(–0.25)

[a] Spectra were recorded in deuteriochloroform at 298 K. [b] Spectra were recorded in dimethylformamide-d_7 (DMF) at 298 K using DMF as a reference (δ 2.76 ppm). Porphyrin concentration was approximately 17 mM. [c] Upon complex formation, the methylene quartet becomes split into two multiplets (see text). [d] Values in parentheses represent differences in chemical shift (Δδ) between complexed and uncomplexed host and guest. [e] Porphyrin concentration was 11 mM.

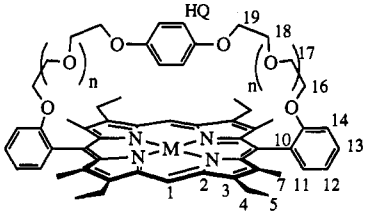

	M	n
8:	2H	1
9:	Zn	1
10:	2H	2
11:	Zn	2

Figure 2. Numbering system employed for the description of NMR resonances of the crown ether strapped porphyrins. For **10** and **11**, the two additional methylene positions in the ether chain are numbered 20 and 21.

BPP34C10 would thus contain a hydroquinol ring centrally located within an ether chain that straps the porphyrin macrocycle, exemplified by **8**. If successful complexation of paraquat by porphyrinic hosts of this type could be ascertained, then this should allow entry to the template-directed synthesis of the corresponding porphyrinic [2]-catenane **17**.

Herein we report the successful synthesis of several porphyrins containing both hydroquinol and naphthoquinol crown ether derived straps, along with their complexation behavior toward paraquat and their subsequent conversion into [2]-catenanes. The methods employed for [2]-catenane synthesis reveal how self-assembly processes, and in particular a template-directed approach, allow a direct entry to the synthesis of these and related molecules.

Results and Discussion

Strapped Porphyrins. The strapped porphyrin formally analogous to BPP34C10 would contain a hydroquinol ring centrally positioned between tetraethylene glycol ether chains. However, molecular modeling indicated that a diethylene glycol chain could provide the approximate 7-Å separation[41] (albeit in an extended conformation) between hydroquinol and porphyrin rings, optimal for paraquat complexation. The increased flexibility provided by triethylene glycol based ether chains, on the other hand, would apparently allow enough freedom for the ether strap to attain the desired 7-Å interaromatic separation without restriction. Thus the porphyrins **8** and **10** (Scheme 1), containing diethylene and triethylene glycol based ethers, respectively, were identified as suitable precursors to [2]-catenane formation.

Scheme 1

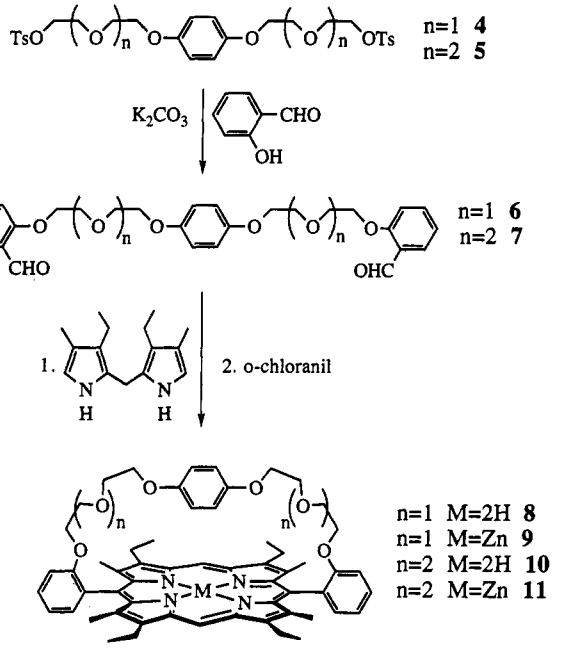

The general scheme for the synthesis of these strapped porphyrins is shown in Scheme 1. The tosylated hydroquinol ether chain derivatives **4** and **5** were allowed to react with salicylaldehyde in acetonitrile with potassium carbonate, yielding **6** and **7**, respectively. These dialdehydes were then condensed with (3,3′-diethyl-4,4′-dimethyl-2,2′-dipyrryl)methane[42] in acetonitrile using trichloroacetic acid catalysis,[43] followed by oxidation of the porphyrinogen with *o*-chloranil,[44] to produce the porphyrins **8** and **10**. Insertion of zinc (zinc acetate/chloroform/methanol) resulted in the corresponding derivatives **9** and **11**. Product verification was carried out by ^{1}H NMR, ^{13}C NMR, and FAB-MS.

A representative example of the ^{1}H NMR resonances of the hydroquinol-strapped porphyrins is collected in Table 1. The nonsystematic numbering system employed in Table 1 is described in Figure 2 and uses the symmetry of the molecule to simplify resonance designations. Proton resonances were assigned using

(41) Such a distance has been identified as being optimal for the complexation of paraquat, as a result of the preferred 3.5-Å separation between interacting rings for effective π–π charge-transfer stabilization.

(42) Young, R.; Chang, C. K. *J. Am. Chem. Soc.* **1985**, *107*, 898–909.
(43) Osuka, A.; Nagata, T.; Kobayashi, F.; Maruyama, K. *J. Heterocycl. Chem.* **1990**, *27*, 1657–1659.
(44) Gunter, M. J.; Mander, L. N. *J. Org. Chem.* **1981**, *46*, 4792–4794.

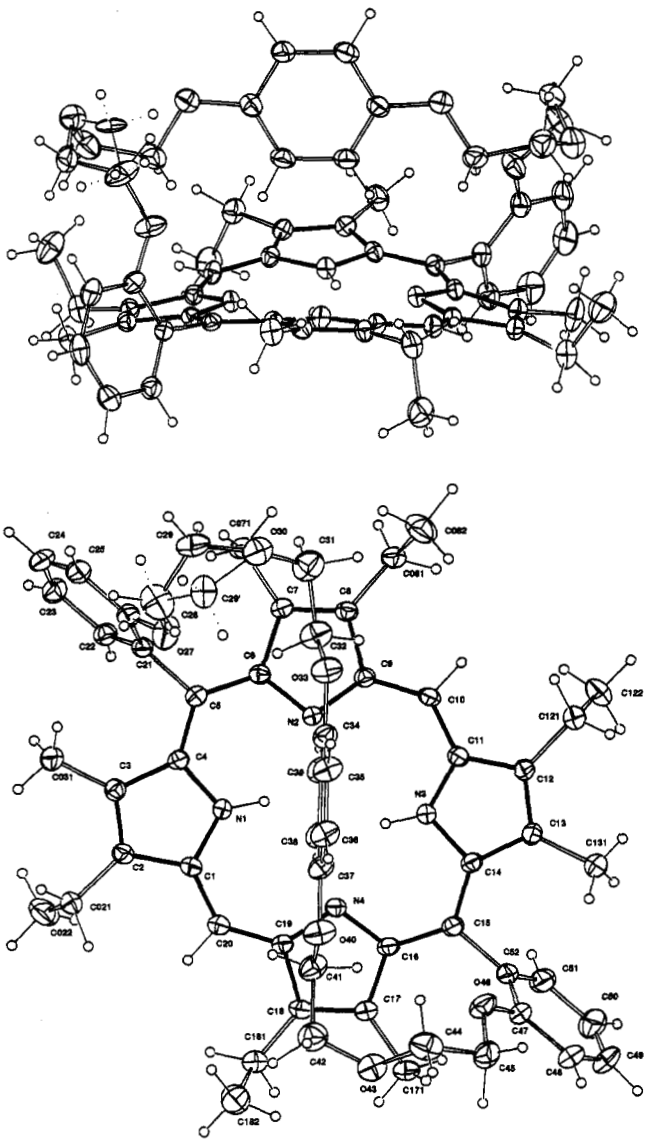

Figure 3. Molecule of **8** projected normal and oblique to the porphyrin plane. Thermal ellipsoids (20%) are shown for the non-hydrogen atoms; hydrogen atoms have arbitrary radii of 0.1 Å.

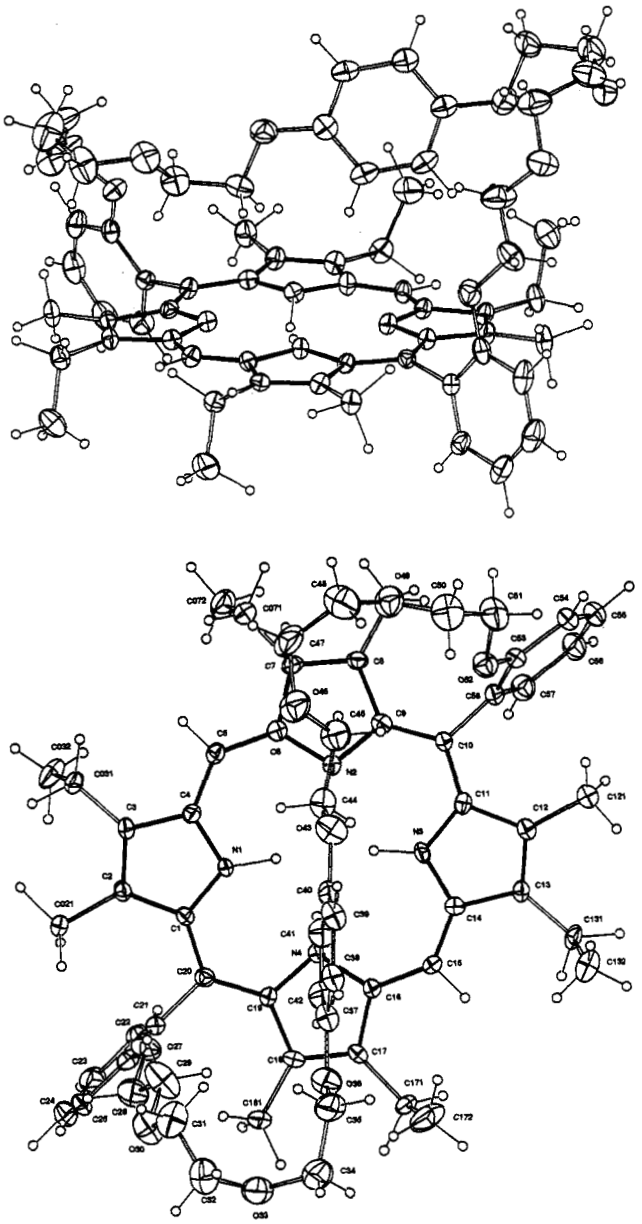

Figure 4. Molecule of **10** projected normal and oblique to the porphyrin plane. Thermal ellipsoids (20%) are shown for the non-hydrogen atoms; hydrogen atoms have arbitrary radii of 0.1 Å.

a combination of COSY-45 and NOE difference spectroscopy. In particular, NOE interactions were observed between protons at the extremities of the ether chains and those of the particular aromatic ring to which the chains are attached.

The chemical shifts for the ether chain and hydroquinol ring protons upon porphyrin formation (Table 1) are indicative of the ether chain strapping the porphyrin ring. For example, in **8**, compared to the open chain hydroquinol crown ether from which it was formed, the difference in chemical shifts of the resonances for H19 and the hydroquinol ring protons HQ ($\Delta\delta$ −2.34 and −3.03 ppm) compared to H16 and -17 ($\Delta\delta$ +0.66 and −0.30 ppm) reflects the more centralized position of the former protons in relation to the porphyrin nucleus and hence a larger effect by the porphyrin magnetic anisotropy. Similar trends can be seen in the other derivatives **9**, **10**, and **11**. The lack of inequivalence within the hydroquinol ring protons in all the strapped porphyrins indicates rapid rotation of the ring about the OC_6H_4O axis in solution.

There are however several differences between the ^1H NMR spectra of **8** and **10**. Firstly, the hydroquinol ring protons of **10** resonate downfield (δ 5.48) in comparison to those of **8** (δ 3.83) as a result of the increased distance of the hydroquinol ring from the porphyrin allowed by the longer triethylene chains in **10**. Secondly, the porphyrin ethyl group resonances for **8** are typical of those usually observed, consisting of well-defined triplet and quartet resonances. However, in the spectrum of **10**, the quartet has been replaced by a multiplet and the triplet is slightly unsymmetrical, indicative of methylene proton diastereotopicity resulting from the asymmetry between the two faces of the porphyrin[45] due to the ether strap. For the methylene resonances, their frequency separation ($\delta\nu$) is much smaller than $J_{geminal}$ (typically 14 Hz), resulting in the multiplet observed.

Solid-State Structures. Single crystals of **8** and **10** suitable for an X-ray crystallographic structure determination were grown from dichloromethane/methanol and yielded the structures shown in Figures 3 and 4.[46] In both cases the hydroquinol ring adopts an essentially orthogonal orientation relative to the porphyrin mean plane (phenyl–porphyrin dihedral angles of 86.7(1) and 83.3(8)°, respectively) in an edge-to-face or T-type geometry which has been observed with many other aromatic systems.[34,47-49] There are close contacts between the electron-rich hydroquinol

(45) Abraham, R. J.; Barnett, G. H.; Smith, K. M. *J. Chem. Soc., Perkin Trans. 1* **1973**, 2142–2148.

C–H and the π-electron cloud of the porphyrin in each case. A face-to-face π-stacked geometry is presumably avoided because of possible repulsive interactions from the electron-rich atoms of the hydroquinol and the porphyrin at the site of contact.[50]

In the structure of **8** (Figure 3), quite severe deformation of the porphyrin skeleton from planarity is evident, forming a typical saddle conformation[51,52] with the pyrrole rings which are aligned with the hydroquinol ring being forced downward below the mean plane of the porphyrin core and the other two pyrroles equally distorted upward from the mean plane. The hydroquinol ring is located almost centrally over the porphyrin and is aligned directly along a N–N axis (H38···N4 and H39···N2 distances are 2.67(3) and 2.46(4) Å, respectively). The ethyl groups on the porphyrin periphery are alternately directed up and down with respect to the porphyrin mean plane.

In contrast, the solid-state structure of **10** (Figure 4) reveals an essentially planar porphyrin skeleton, indicating less constraint by the looser strap, and ethyl substituents on opposite sides of the porphyrin ring having different orientations, either up or down. In common with **8**, however, the *meso*-phenyl rings of **10** are twisted in opposite directions with respect to each other away from complete orthogonality with the porphyrin plane. It is interesting to note that, in **10**, the hydroquinol ring is not centrally located over the porphyrin macrocycle, although it is still aligned along a N···N axis. It is now virtually directly located above a pyrrole nitrogen atom, and the lower edge is not parallel to the mean porphyrin plane but is tilted significantly. However, it is evident that a T-type π–π interaction is maintained (H41···N4 distance of 2.8$_4$ Å).

These structures imply that **8** and **10** both adopt a self-filling structure in the solid state, which if retained in solution may be detrimental to paraquat complexation since host reorganization would be necessary. However, since the ^{1}H NMR spectrum does not reveal any inequivalence within the hydroquinol protons, fast rotation of the ring must occur in solution, and the π–π interaction is maintained.

Paraquat Complexation. In order for the strapped porphyrins **8** and **10** and their corresponding zinc derivatives **9** and **11** to be incorporated into [2]-catenanes by template-directed synthesis, they must necessarily complex the paraquat dication in a manner analogous to that for BPP34C10 (Figure 1). Evidence for such complexations resulted from an examination of the ^{1}H NMR spectra of equimolar solutions of either **9** or **11**[53] and paraquat in DMF-d_7. An example of the complexation-induced shifts

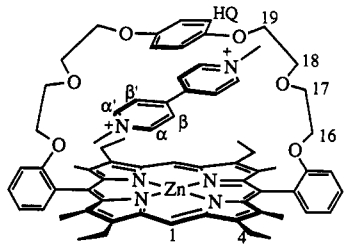

9.PQ^{2+}

Figure 5. Complexation geometry of paraquat within **9** deduced from ^{1}H NMR studies.

observed for these complexations is shown in Table 1. These shifts support an inclusion complex structure as indicated in Figure 5, containing hydroquinol, paraquat, and porphyrin rings coparallel. This is indicated by several factors. Firstly, upfield shifts were observed for both resonances of groups on the porphyrin periphery (in particular H1 Δδ –0.22 for **9**), along with the paraquat guest resonances. Within the paraquat resonances, the larger shifts observed for the resonances of β,β′-protons (Δδ –0.96 ppm), in comparison to the α,α′-protons (Δδ –0.54 ppm) and $^+$N–Me protons (Δδ –0.30 ppm), reflect the closer proximity of the former to the center of the porphyrin ring (Figure 5). Secondly, there are complexation-induced changes to resonances of the ether moiety, albeit complicated by a conformational change; the hydroquinol ring is forced away from the porphyrin nucleus, resulting in a deshielding of its protons along with those of the ether chain. The inclusion of paraquat then counteracts this change by shielding the hydroquinol protons yet reinforces the change by deshielding the ether protons to produce the shifts observed (Table 1).[54]

An unusual complexation-induced effect is also observed within the porphyrin ethyl group resonances. The usual coupling pattern observed in the ^{1}H NMR spectrum of **9** consists of well-defined triplet and quartet resonances; however, in the spectra of **9**/PQ^{2+} and **11**/PQ^{2+}, the methylene quartet and multiplets have been replaced by two multiplets and the triplet is slightly unsymmetrical as a result of methylene and methyl proton diastereopicity[55] resulting from the influence of the complexed paraquat magnetic anisotropy. Thus the methylene proton resonances have an additional multiplicity resulting from geminal coupling, typically 14 Hz. In the case of **9**/PQ^{2+}, the frequency separation ($\delta\nu$) between the methylene resonances results in the observation of

(46) Structure determinations. **8**: $C_{58}H_{64}N_4O_6{\cdot}CH_2Cl_2$; triclinic, $P\bar{1}$, a = 15.264(2), Å, b = 13.518(6) Å, c = 13.424(2) Å, α = 87.96(3)°, β = 85.36-(1)°, γ = 69.91(2)°, V = 2593 Å^3, D_c (Z = 2) = 1.28 g cm^{-3}; monochromatic Mo $K\alpha$ radiation, λ = 0.7107$_3$ Å; N_0 = 4175 unique diffractometer data ($2\theta_{max}$ = 50°) (no absorption correction) refined to R = 0.049, R_w (statistical weights) = 0.048 on $|F|$ (full matrix least squares anisotropic thermal parameter refinement for C, N, O, Cl; (x, y, z, U_{iso})$_H$ ordered components). In the ligand, C29 was modeled as disordered equally over two sites; the solvent was described in terms of three equally populated disordered pairs of chlorine atoms disposed about a central carbon, assigned as CH_2Cl_2 rather than $CHCl_3$ disordered over two sites on historical grounds and site occupancy refinement. **10**: $C_{62}H_{72}N_4O_8{\cdot}0.5CH_3OH$; triclinic, $P\bar{1}$, a = 16.50(2) Å, b = 13.92(1) Å, c = 12.150(6) Å, α = 79.75(6)°, β = 87.19(6)°, γ = 77.97(7)°, V = 2685 Å^3, D_c (Z = 2) = 1.26 g cm^{-3}; R, R_w = 0.060, 0.053 for N_0 = 2819 ($2\theta_{max}$ = 50°, although data weaker than for **8** on account of small crystal size). The solvent molecule is modeled as disordered about a center of symmetry; (x, y, z, U_{iso})$_H$ were constrained estimates.

(47) Burley, S. K.; Petsko, G. A. *Science* **1985**, *229*, 23–28.

(48) Burley, S. K.; Petsko, G. A. *J. Am. Chem. Soc.* **1986**, *108*, 7995–8001.

(49) Cochran, J. E.; Parrott, T. J.; Whitlock, B. J.; Whitlock, H. W. *J. Am. Chem. Soc.* **1992**, *114*, 2269–2270.

(50) For a discussion and rationalization of the factors influencing the geometry of π–π interactions, see: Hunter C. A.; Sanders, J. K. M. *J. Am. Chem. Soc.* **1990**, *112*, 5525–5534.

(51) Barkigia, K. M.; Berber, M. D.; Fajer, J.; Medforth, C. J.; Renner, M. W.; Smith, K. M. *J. Am. Chem. Soc.* **1990**, *112*, 8851–8857.

(52) Medforth, C. J.; Berber, M. D.; Smith, K. M.; Shelnutt, J. A. *Tetrahedron Lett* **1990**, *31*, 3719–3722.

(53) Complexation studies were undertaken with the metalated derivatives **9** and **11** due to the limited solubility of the free base forms in most polar organic solvents.

(54) The larger shifts observed for the hydroquinol and adjacent methylene protons in **9**/PQ^{2+} compared to **11**/PQ^{2+} are a result of the stronger shielding of these protons in the tighter strap derivative before complexation. In the complexes, it is expected that the porphyrin–paraquat–hydroquinol separations would be similar in each case. However, the difference in chemical shifts on complexation will also be influenced by any change in the extent of buckling of the porphyrin, especially in the tight strap (evident in the solid-state structure and which is also manifest in the larger change for the *meso*-protons H1), and the fact that at these concentrations the paraquat is only about 80% bound in each case, so that the observed chemical shifts are averages of the bound and unbound values. The observed complexation here is in apparent conflict with the lack of interaction observed between the dication and porphyrin moieties in a previously reported paraquat-strapped porphyrin (Leighton, P.; Sanders, J. K. M. *J. Chem. Soc., Chem. Commun.* **1984**, 856–857). Likewise, no evidence for direct porphyrin–bipyridinium electronic interaction was observed in a series of porphyrins with appended bipyridinium receptor sites (Gunter, M. J.; Johnston, M. R. *Tetrahedron Lett.* **1990**, *31*, 4801–4804. Gunter, M. J.; Johnston, M. R. *Tetrahedron Lett.* **1992**, *33*, 1771–1774), or in the analogous unstrapped 2,8,13,18-tetraethyl-3,7,14,17-tetramethyl-5,-15-diphenylporphyrin. However, it is clear that, in the case of **9** and **11**, the additional influence of the hydroquinol ring allows electronic interaction between the porphyrin and paraquat and that the shifts in the proton resonances for the paraquat in each case cannot be explained simply by π–π interactions at the unstrapped face of the porphyrin.

(55) If such an effect were due to ethyl *group* diastereotopicity, rather than from *within* a particular methylene group, as suggested by the crystal structure of **8** shown in Figure 3, then a splitting of both quartets and their corresponding triplets would be expected. The two spin systems thus created, consisting of two quartets and two triplets, would not interact via scalar coupling as is observed within the multiplet signals of **9** upon paraquat complexation.

Scheme 2

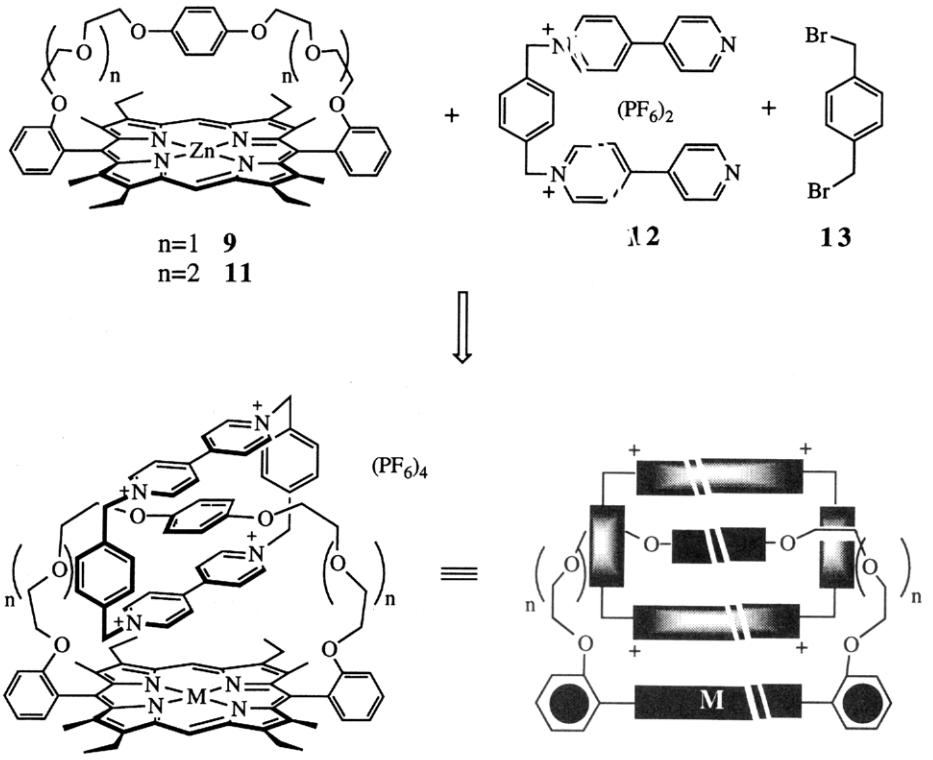

n=1 **9**
n=2 **11**

12 **13**

n=1 M=Zn **14**
n=1 M=2H **15**
n=2 M=Zn **16**
n=2 M=2H **17**

second-order effects in the spectrum. The asymmetry of the triplet resonance reflects the small influence of the paraquat anisotropy on the methyl protons such that $(\delta\nu) < J_{AB}$.

The addition of paraquat to solutions of the strapped porphyrins had little effect on the Soret absorptions in the UV spectra, and yet the NMR evidence is for a complex with the hydroquinol, paraquat, and porphyrin rings parallel and involving mutual π–π interactions. This apparent anomaly may be explained as follows: the π–π interactions (edge-to-face) that characterize the solid-state structures might reasonably be expected to be maintained in solution (although obviously with free rotation of the hydroquinol ring). This would be manifested by a red shift of the Soret bands compared to those of the unstrapped analogues, and indeed the Soret bands for the strapped porphyrins are at a 6-nm longer wavelength than those for the zinc complex of the analogous unstrapped 2,8,13,18-tetraethyl-3,7,14,17-tetramethyl-5,15-diphenylporphyrin.[56] Thus the lack of spectral changes upon paraquat addition may be interpreted as a replacement of the hydroquinol π-system by that of the paraquat in interaction with the porphyrin.

Association constants for the complexation of paraquat by the hydroquinol-strapped porphyrins were determined using ^{1}H NMR spectroscopy.[57] In the case of **9**/PQ^{2+}, an association constant K_a of 1.95×10^3 M^{-1} at 298 K was determined, with an associated free energy of complexation $\Delta G°$ of –4.5 kcal mol^{-1}. The triethylene glycol strapped porphyrin **11** was found to have a K_a of 1.64×10^3 M^{-1} at the same temperature, with a $\Delta G°$ of –4.4 kcal mol^{-1}. The approximately equal complexation strengths of **9** and **11** are not unexpected since the dication is sandwiched between hydroquinol and porphyrin rings in both complexes. Both complexations are stronger than that observed with BPP34C10 (K_a = 730 M^{-1}, $\Delta G°$ = –3.9 kcal mol^{-1})[38] as well as that with 1,5-DN38C10 (K_a = 317 M^{-1}, $\Delta G°$ = –3.41 kcal mol^{-1})[40] and reflect the enhanced interaction between the more π-electron-rich subunits of **9** and **11** and the π-electron-deficient bipyridinium dication. With the complexation geometry in these molecules thus established (Figure 5), the template-directed synthesis of [2]-catenanes could now be addressed, as outlined by the strategy depicted in Figure 1.

[2]-Catenane Self-Assemblies. The chosen route to the catenanes was *via* the clipping strategy[2,37] developed by Stoddart for the analogous bis(phenylene)crown ethers such as BPP34C10. This procedure relies on the directed attractive forces between the components during the assembly process and especially on π–π interactions between the π-electron-rich hydroquinol and the π-electron-deficient aromatic rings of the bipyridinium derivatives, both of paraquat in the first instance and of the tetracationic cyclophane **1** in the final product. Such a template-directed synthesis utilizes the mutual complexing properties of the two components of the catenane for efficient synthesis. The analogous procedure for [2]-catenane formation based on the hydroquinol-strapped porphyrins is outlined in Scheme 2 and involves the reaction of the bis(bipyridinium)cyclophane[58] **12**, 1,4-bis(bromomethyl)benzene **13**, and the hydroquinol-strapped porphyrins **9** or **11** in dimethylformamide at room temperature for 7 days. Subsequent chromatography and anion exchange produced the [2]-catenanes **14** and **16** in 20 and 28% yields, respectively. The zinc free derivatives **15** and **17** were obtained by treatment of **14** and **16** with aqueous hydrochloric acid followed by neutralization and anion exchange.[59]

The [2]-catenanes produced were analyzed by positive ion FAB-MS in the first instance. Peaks were observed for the parent ion,

(56) Robinson, B. C. Ph.D Thesis, University of New England, Armidale, Australia, 1991.

(57) The method employed involves the measurement of complexation-induced shifts ($\Delta\delta_{obs}$) for various resonances with successive dilution of an equimolar solution of host and guest. A linear plot of $\Delta\delta_{obs}$ against $\Delta\delta_{obs}$/[conc] then allows the association constant (K_a) to be determined.

(58) Geuder, W.; Hünig, S.; Suchy, A. *Tetrahedron* **1986**, *42*, 1665–1677.

Table 2. Selected ^{1}H NMR Resonances (δ, ppm) and Chemical Shift Differences ($\Delta\delta$, ppm) for Catenanes and Their Component Parts

	α	β	$-C_6H_4-$	$^+NCH_2$	HQ
1[a]	8.86	8.16	7.52	5.74	6.73[b]
[2]-catenane **3**[a]	8.85	7.66	7.79	5.67	3.45
$\Delta\delta$[c]	(–0.01)	(–0.50)	(+0.27)	(–0.07)	(–3.28)
9					3.83[d]
[2]-catenane **14**[e]	8.06	5.87	7.46	5.28,	2.44
$\Delta\delta$[c]	(–0.80)	(–2.29)	(–0.06)	(–0.4 6)	(–1.39)
[2]-catenane **16**[f]	7.80	5.76	7.37	5.26	2.59
$\Delta\delta$[c]	(–1.06)	(–2.40)	(–0.15)	(–0 .48)	(–2.89)

[a] Data is from Stoddart *et al.*[2] [b] Hydroquinol ring proton chemical shift before catenane formation is from BPP34C10.[2] [c] $\Delta\delta$ represents the change in chemical shift on formation of the catenane from its component parts, *viz.* **1** and the appropriate crown ether **2** or strapped porphyrin **9** or **11**. [d] In $CDCl_3$ at 25 °C. [e] Spectrum recorded in DMSO at 105 °C under conditions of fast exchange (see text). [f] Spectrum recorded in CD_3CN at 70 °C.

as well as the loss of one, two, and three PF_6^- counterions typical of the behavior of non-porphyrinic catenanes.[2] In the case of **14** and **16**, peaks for each counterion loss were accompanied by peaks corresponding to the removal of zinc from the porphyrin. After loss of the third anion, the next highest mass peaks observed in the spectra were those from the corresponding parent porphyrin resulting from the unthreading of the tetracationic macrocycle **1**.

The porphyrin [2]-catenanes were also thoroughly investigated by ^{1}H NMR spectroscopy. By way of example, selected resonances of **14**, recorded under conditions of fast exchange (see below), are collected in Table 2 along with various data from non-porphyrinic catenanes. For all resonances, an increased change in chemical shift between **1** and **14** is observed in comparison to those of the BPP34C10-based [2]-catenane **3**, owing to the large magnetic anisotropy of the porphyrin ring. The complexed hydroquinol ring proton resonance shifts upon catenane formation in **14** are complicated by a conformational change in which the hydroquinol ring is moved away from the porphyrin nucleus, analogous to that observed earlier for paraquat complexation. However, when the effects of shielding by the porphyrin and this conformation change are taken into account, the complexed hydroquinol ring proton resonances undergo similar changes upon catenane formation for **3** and **9** ($\Delta\delta$ –3.28 and –1.39 ppm, respectively), indicating an inclusion geometry within the tetracationic macrocycle **1** analogous to that in the non-porphyrinic catenanes.

The diastereotopicity within the porphyrin methylene protons upon paraquat complexation is again evident in the catenane ^{1}H NMR spectra. However, the permanent presence of the tetracation in the catenane structures increases the chemical shift differences between methylene proton environments ($\Delta\delta$ 0.39 ppm in the case of **9**) over that observed for paraquat complexation ($\Delta\delta$ 0.16 ppm). A successful PANIC[60] simulation of the $ABCX_3$ coupling pattern provided additional proof of the diastereotopic nature of the methylene protons, revealing $J_{vicinal}$ = 7.5 Hz and $J_{geminal}$ = 14.3 Hz.

It was reasoned that there were two possible extremes for the relative orientations of the components within porphyrin [2]-catenanes, depicted in Figure 6. If the hydroquinol ring were orthogonal to the porphyrin, as is the case in the solid state (see Figures 3 and 4), then there would be no porphyrin–bipyridinium

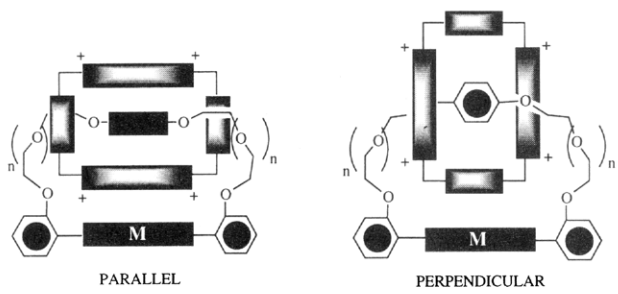

Figure 6. Schematic representation of the two possible conformational extremes of the catenane, showing the relative orientations of the hydroquinol and porphyrin rings, and the tetracationic macrocycle.

interaction (a reasonable possibility, see ref 54) and the catenane would exhibit π–π interactions only between the hydroquinol and the tetracation; in this case, the phenylene moiety of the tetracationic macrocycle would be closest to the porphyrin, as shown in Figure 6. On the other hand, if there were significant charge-transfer interactions between the porphyrin and the bipyridinium macrocycle, the hydroquinol and porphyrin rings would be parallel and the "sandwiched" bipyridinium moiety would be nearest the porphyrin. The conformation shown in Scheme 1, and depicted as the "parallel" orientation in Figure 6 with the bipyridinium, hydroquinol, and porphyrin rings coparallel, was deduced from the ^{1}H NMR data. The data shown in Table 2, collected under fast exchange conditions (see below and Figure 8), reveal that the β-bipyridinium resonances are most affected by catenane formation ($\Delta\delta$ –2.29 ppm). Additionally, under conditions of slow exchange (see the dynamic NMR discussion below and Table 3), the β-proton resonances of **14** are split into two peaks with a remarkably large separation ($\Delta\delta$ 3.70 ppm). The next largest separation between resonances occurs for the α-protons ($\Delta\delta$ 1.67 ppm), while the phenylene protons show only minimal splitting. This indicates a conformation in which the bipyridinium moiety is closest to, and hence most affected by, the porphyrin. Such a conformation intuitively follows from the geometry of the inclusion complex formed between the strapped porphyrins and the paraquat dication observed earlier, in which the π-electron-deficient guest is sandwiched parallel between the π-electron-rich porphyrin and hydroquinol rings.

The existence of π–π electron charge-transfer interactions between the bipyridinium moiety of the tetracationic macrocycle **1** and the porphyrin nucleus could not be directly observed by UV/visible spectroscopy since the large porphyrin Soret band obscures any charge-transfer absorption band that may be present.[61] However, that there is some electronic interaction is revealed by the changes upon catenane formation of the porphyrin Soret absorption from 414 nm in **9** or **11** to 422 nm in **14** or **16**, with no change occurring for the Q-bands (>450 nm). Control experiments were carried out with **9** in the presence of paraquat, bis(bipyridinium)dication **12**, and separately synthesized tetracationic macrocycle **1**, and in no instance were any significant changes in the absorption spectrum of the porphyrin observed.[62]

Dynamic ^{1}H NMR. An examination of the porphyrin [2]-catenanes by ^{1}H NMR spectroscopy revealed considerable temperature dependence. The ^{1}H NMR resonances at various temperatures were assigned using a combination of saturation transfer, NOE difference, and COSY-45 spectroscopy. In particular, NOE interactions were observed both within the tetracationic macrocycle and between the tetracation and the hydroquinol ether protons, confirming the inclusion of the hydroquinol ring within the macrocycle (Figure 7A,B).

(59) The mechanism for catenane formation is presumably similar to that reported (Philp, D.; Stoddart, J. F. *Synlett* **1991**, 445–458), consisting of an initial nucleophilic attack of **12** on **13** (Scheme 2) to produce an intermediate tricationic species which then spontaneously complexes with the strapped porphyrins in a manner similar to that described for paraquat. A second intramolecular nucleophilic substitution within the complexed tricationic molecule would thus yield the [2]-catenanes.

(60) Parameter Adjustment in NMR by Iteration Calculation, Bruker software.

(61) The expected charge-transfer band ($\lambda \approx 420$ nm, $\epsilon \approx 300$) (Ashton, P. R.; Slawin, A. M. Z.; Spencer, N.; Stoddart, J. F.; Williams, D. J. *J. Chem. Soc., Chem. Commun.* **1987**, 1066) is totally swamped by the porphyrin Soret absorption band ($\lambda \approx 400$–410 nm, $\epsilon \approx 3 \times 10^5$).

Table 3. Chemical Shift Values (ppm) for Selected Protons for the Hydroquinol-Containing Porphyrin [2]-Catenanes **16** and **17** at Several Temperatures

	16			**17**		
^{1}H	fast rotation, CD_3CN, +70 °C	slow rotation, acetone-d_6, −40 °C	$\Delta\delta^c$	fast rotation, CD_3CN, 70 °C	slow rotation, acetone-d_6, −35 °C	$\Delta\delta^c$
α	7.80	"outside" 8.99 "inside" 7.62	1.37	7.83	"outside" 8.48 "inside" 7.15	1.33
β	5.76	"outside" 7.86 "inside" 3.74 (hidden)^b	4.12	5.82	"outside" 7.42 "inside" 3.53 (hidden)^b	3.89
$-C_6H_4-$	7.37	7.71 7.52	0.19	7.39	7.42 7.32	0.10
$^+NCH_2$	5.27	5.82 5.67	0.15	5.27	5.41 5.22	0.19
HQ	2.59	*a*		2.62	*a*	

[a] Hydroquinol ring proton resonances are broadened under slow exchange and are not visible. [b] Located using saturation transfer techniques. [c] Chemical shift differences between protons in slow exchange environments.

An example of the temperature dependence of the ^{1}H NMR spectra of the porphyrin catenanes is shown in Figure 8, with spectra of **17** in CD_3CN at high and low temperatures. The results from this and other dynamic ^{1}H NMR spectra of **16** and **17** are collected in Table 3.

At 45 °C, the ^{1}H NMR spectrum of **17** reveals single peaks for all resonances of the tetracation (Figure 8). However, at temperatures below 45 °C, the resonances of the tetracation split into equal intensity peaks reflecting different environments of these protons within the catenane.[63] These results may be interpreted as the dynamic behavior of the tetracation illustrated in Figure 9 and result from the interchange of the bipyridinium rings (A and B) between the "inside" and "outside" environments.[19] This interchange may be regarded as the tetracation *rotating* about an axis created by the hydroquinol ring.[64] The observable splitting of the tetracation resonances at lower temperatures (Table 3) indicates slowing of the rotation of the macrocycle on the NMR time scale.

The resonances of the porphyrin moieties within the catenanes exhibit no dynamic behavior, since each position of the tetracation (i.e. whether ring A or B is "inside" or "outside") (Figure 9) does not effect the porphyrin environment. An increase in temperature fails to coalesce the methylene multiplets, reinforcing the assertion that such splitting occurs *within* each methylene group rather than as a result of ethyl *group* diastereotopicity, which has been found to be temperature dependent.[51,52]

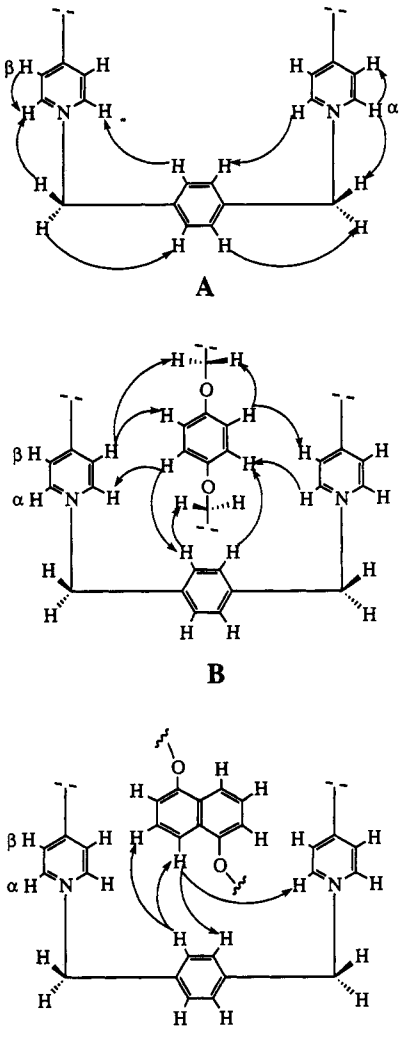

Figure 7. NOE interactions observed in the catenanes: (A) interactions within the tetracationic macrocycle of the catenanes, measured under conditions of slow or fast exchange; (B) interactions between the tetracationic macrocycle and the hydroquinol and ether chain protons in **17** under fast exchange conditions (45 °C, CD_3CN); (C) interactions between the tetracation and the naphthalene protons in **23** under slow exchange conditions (−35 °C, CD_3CN).

Rotation rates of the tetracationic macrocycle within the various catenanes were measured using the coalescence method[65] by following the methylene protons (δ = 5.5 ppm), since these provided the most accessible probe (Table 4). For example, in the case of **14**, a $\delta\nu$ of 200.5 Hz at a T_c of 43 °C in acetone yielded

(62) The red shift in the porphyrin Soret absorption originates from the stabilization of the porphyrin HOMO molecular orbitals a_{1u} and a_{2u} (and/or $e_g(\pi^*)$ (LUMO) destabilization). However, the problem lies in identifying the actual mechanism by which these orbitals are stabilized. This red shift of the porphyrin Soret band ($\Delta\lambda$ 8 nm) may be due to several possible factors acting independently or in some combination. Firstly, the shift may be an interaction of the π-electron systems of the bipyridinium subunits of the tetracation and the porphyrin (Shelnutt, J. A. *J. Phys. Chem.* **1984**, *88*, 6121–6127) with the larger change observable in the [2]-catenane over that for paraquat complexation due to the permanent presence of the bipyridinium rings in the catenane. Secondly, the presence of the positive charges of the tetracation in close proximity to the porphyrin may perturb the porphyrin electronic structure, resulting in absorption spectrum changes (Gudowska-Nowak, E.; Newton, M. D.; Fajer, J. *J. Phys. Chem.* **1990**, *94*, 5795–5801). Thirdly, there may be a steric interaction between the large tetracation and the porphyrin which results in a perturbation of the electronic structure of the porphyrin without deformation of the porphyrin skeleton (puckering of the porphyrin has the effect of red shifting all the porphyrin absorptions by 4–12 nm as a result of $e_g(\pi^*)$ orbital stabilization (Simonis, U.; Walker, F. A.; Lani Lee, P.; Hanquet, B. J.; Meyerhoff, D. J.; Scheidt, R. W. *J. Am. Chem. Soc.* **1987**, *109*, 2659–2668), whereas catenane formation is observed to shift only the Soret band). The precise nature, however, of the origin of the red shift of the Soret upon catenane formation could not be determined from the evidence available.

(63) Temperature reduction also has the effect of broadening the hydroquinol resonance. This has been attributed to "rocking" of the hydroquinol ring between two orientations within the tetracation.[2]

(64) The dynamic process within the porphyrin catenanes is simpler than those processes observed in the non-porphyrinic [2]-catenane **3**, since although tetracation macrocycle rotation (or "pirouetting" of the crown ether)[19] is observed, the process equivalent to "threading" of the crown ether through the macrocycle in **3** is clearly disallowed in this case because of the bulky porphyrin moiety.

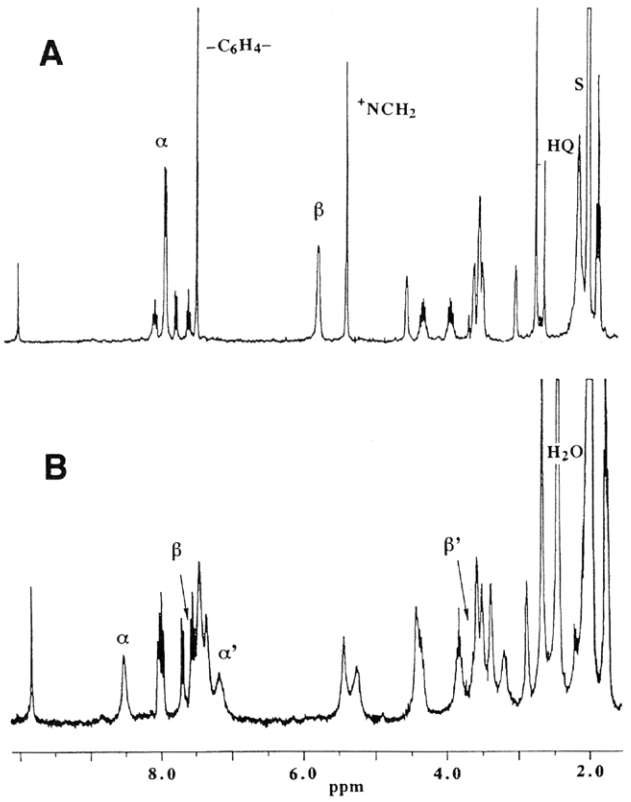

Figure 8. Partial ^{1}H NMR spectra at 300 MHz for **17** in CD_3CN at (A) 45 °C and (B) −35 °C, revealing fast and slow tetracation rotation, respectively. At −35 °C, the splitting of tetracation resonances is clearly evident and allows the observation of the "inside" and "outside" bipyridinium environments. Clearly visible in the fast exchange spectrum are the diastereotopic methylene multiplet resonances $\delta \approx 3.9$ and 4.3 ppm.

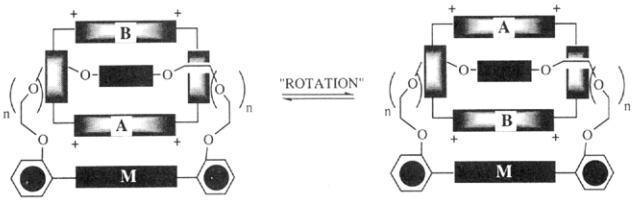

Figure 9. Schematic representation of the dynamic behavior of the tetracationic moiety of the porphyrin [2]-catenanes. The exchange of rings A and B between "inside" and "outside" environments may be regarded as *rotation* of the tetracation.

$k_c = 445$ s^{-1} with a $\Delta G_c^{\ddagger}$ of 14.7 kcal mol^{-1}. Thus, at ambient temperature, the tetracationic macrocycle rotates at 50 times per second.

The rotation rates for the diethylene glycol containing catenanes are very slow in comparison with the BPP34C10-based catenane **3** (Table 4), in which the macrocycle rotates at 2000 times per second with a $\Delta G_c^{\ddagger}$ of 12.2 kcal mol^{-1}.[37] The larger $\Delta G_c^{\ddagger}$ observed for both **14** and **15** (Table 4) may be interpreted as a larger energy barrier to macrocycle rotation within these catenanes, necessarily resulting in the slower rates observed. This larger $\Delta G_c^{\ddagger}$ may result from a steric, or electronic, interaction (or a combination of both) between the tetracation and the porphyrin nucleus. However, the similarity between rotation rates and $\Delta G_c^{\ddagger}$ values for the BPP34C10-based catenane and those of the porphyrin catenanes containing the triethylene glycol thread **16** and **17**, together with the fact that there is little difference between **14** and **16** or **15** and **17** in the electronic interactions of macrocycle and porphyrin, imply that the slower rates for **14** and **15** result from purely steric constraints; the short nature of the hydroquinol ether strap provides a significant steric barrier to rotation of the rectangularly-shaped tetracation.

(65) The coalescence method (Sandström, J. *Dynamic NMR Spectroscopy*; Academic Press: New York, 1982; Chapter 6) uses the expression $k_c = \pi(\delta\nu)/2^{1/2}$ to approximate the rotation rate at the coalescence temperature T_c. The linear temperature dependence of the frequency separation ($\delta\nu$) was measured in the slow exchange region and extrapolated to T_c. The errors associated with rates measured in this manner are on the order of 20% (Sutherland, I. O. *Annu. Rep. NMR Spectrosc.* **1971**, *4*, 71–235. Kost, D.; Carlson, E. H.; Raban, M. *J. Chem. Soc., Chem. Commun.* **1971**, 656–657). Free energy of activation $\Delta G_c^{\ddagger}$ was then determined with the Eyring equation, and the van't Hoff equation was subsequently applied for the conversion of rotation rates to those at 298 K.

Table 4. Kinetic and Thermodynamic Parameters from the Dynamic ^{1}H NMR Studies on the Porphyrin Catenanes for Tetracation Rotation[a]

catenane	$\Delta\nu$ (Hz)	T_c (°C)	k_c (s^{-1})	rotation rates at 25 °C (Hz)	$\Delta G_c^{\ddagger}$ (kcal mol^{-1})
3[b] (BPP34C10 catenane)				2000	12.2
14	200.5	+43	445	50	14.7
15	194	+37	431	80	14.4
16	47	−21	104	2500	12.3
17	21.7	−20	68	1500	12.6
23	149	+59	331	10	15.7
24	139	+59	310	10	15.7
1,5DN38C10 catenane[c]				1200	12.7
23[d]	60[d]	+3[d]	134[d]	400[d]	13.4[d]
24[d]	65[d]	−8[d]	145[d]	1000[d]	12.8[d]
1,5DN38C10 catenane[d]				10[d]	15.8[d]

[a] Data obtained by the coalescence method (see ref 65). [b] Data is from the literature.[19,37] [c] Data is from the literature.[19] [d] Refers to the "out, turn around, and in again" process observed in naphthoquinol catenanes.

Naphthoquinol/Porphyrin Catenane. The importance of π–π electron interactions in the formation of inclusion complexes involving BPP34C10 led to the subsequent extension of the concept and the replacement of the π-electron-rich system of the hydroquinol unit in the crown ether with a naphthoquinol.[66] Since we had now demonstrated that the inclusion of a porphyrin macrocycle into a hydroquinol crown ether may result in the formation of porphyrin-containing [2]-catenanes, then likewise, it seemed possible to extend the methodology beyond the hydroquinol porphyrin catenanes by utilizing an increase in π-electron-donating properties of the aromatic ring strapping the porphyrin ring. The obvious choice for a larger π-electron system for inclusion into porphyrin catenanes was thus the 1,5-dihydroxynaphthalene ring, since crown ethers containing naphthalene rings successfully complex paraquat,[66] as well as efficiently form [2]-catenanes.[20] The formation of a porphyrin catenane containing a naphthalene ring would then provide a test of the generality of the synthesis for porphyrin catenanes outlined in Scheme 2.

An examination of molecular models revealed that a naphthalene-containing porphyrin strap incorporation diethylene glycol ether chains, analogous to **8**, would create a sterically crowded environment for both paraquat complexation and catenane formation. However, the use of triethylene glycol ether chains in the porphyrin strap, similar to **10**, would create a cavity suitable for such purposes. Thus a 1,5-disubstituted naphthalene ring subtended by triethylene glycol chains and strapped across a porphyrin was identified as an initial synthetic target.

The synthetic route that yielded the naphthalene-strapped porphyrin **21** is analogous to the general procedure outlined for hydroquinol-strapped porphyrins and is shown in Scheme 3. The naphthalene-strapped porphyrin **21** was produced in 10% yield and its identity verified by ^{1}H and ^{13}C NMR and FAB-MS.

The ^{1}H NMR spectrum of **21** contains resonances of the ether chains that are similar to those observed for the hydroquinol-strapped porphyrin **10**, indicating a similar position of the ether

(66) Ashton, P. R.; Chrystal, E. J. T.; Mathias, J. P.; Parry, K. P.; Slawin, A. M. Z.; Spencer, N.; Stoddart, J. F.; Williams, D. J. *Tetrahedron Lett.* **1987**, *28*, 6367–6370.

Scheme 3

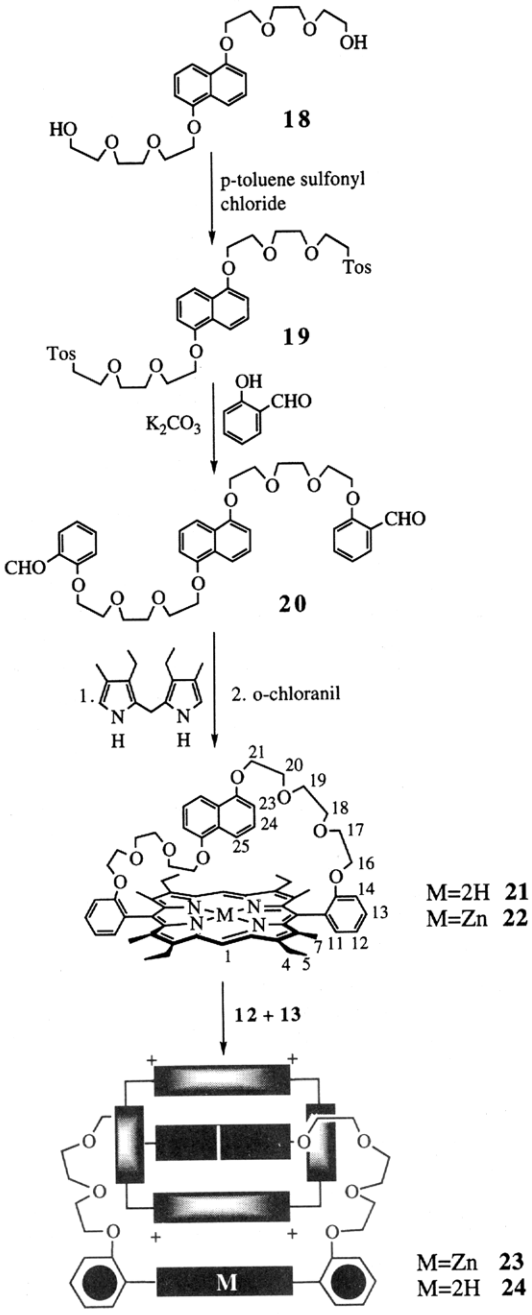

chains relative to the porphyrin plane. Once again these resonances were assigned using a combination of NOE and COSY-45 results.

The complexing ability of **22** toward paraquat was likewise examined by ^{1}H NMR in dimethylformamide-d_7. As expected, the complexation-induced changes to chemical shifts of both the strapped porphyrin and paraquat were consistent with a complexation geometry in which the naphthalene, paraquat, and porphyrin rings are orientated parallel, as observed previously for the hydroquinol-strapped porphyrins and paraquat. In terms of the individual moieties within the inclusion complex, the complexation-induced shifts were qualitatively similar to those outlined above for the complexation of paraquat by **9**. The association constant K_a between **22** and paraquat at 25 °C was determined as 2.11×10^4 M^{-1} with $\Delta G° = -5.9$ kcal mol^{-1}. Such a complexation strength is exceptionally large in comparison to the hydroquinol-strapped porphyrins ($K_a = 1.95 \times 10^3$ M^{-1} and $\Delta G° = -4.5$ kcal mol^{-1} for **9**, $K_a = 1.64 \times 10^3$ M^{-1} and $\Delta G° = -4.5$ kcal mol^{-1} for **11**) and the dinaphthalene crown ether 1,5-DN38C10 ($K_a = 3.75 \times 10^2$ M^{-1}, $\Delta G° = -3.41$ kcal mol^{-1})[40] and reflects the increased interaction between π-electron-rich **22** and the π-electron-deficient paraquat dication. The strength and geometry of paraquat complexation by **22** thus gave a bright prognosis for its incorporation into a [2]-catenane.

The general procedure for the porphyrin-containing [2]-catenane synthesis outlined in Scheme 2 for the hydroquinol-strapped porphyrins was applied to the naphthalene-strapped porphyrin **22**, and the naphthalene-containing [2]-catenane **23** was isolated in 45% yield. The higher yield of **23** over the hydroquinol-based catenanes (**14**, 20%; **16**, 28%) presumably reflects the stronger complexing ability of **22** toward the paraquat derivative within the tricationic intermediate. Subsequent demetalation of **23** with aqueous hydrochloric acid yielded **24**.

The structural verification of the [2]-catenanes **23** and **24** was carried out in the first instance by FAB-MS. In what has now become a familiar pattern, peaks were observed for the loss of one, two, three, and four PF_6^- counterions, with the next lowest peak observed representing the disentanglement of the tetracation **1** from the strapped porphyrin. In the metalated catenane **23**, several additional peaks were also observed, corresponding to the removal of zinc from the porphyrin.

The ^{1}H NMR spectra of **23** and **24** at both high and low temperatures (selected resonances of which are collected in Table 5) were assigned using the previously employed techniques of NOE difference, saturation transfer, and COSY-45 spectroscopy. As was found in the hydroquinol-containing catenanes, NOE interactions were observed both within the tetracation macrocycle and between it and the complexed aromatic ring (Figure 7C). The slow exchange data in Table 5 imply a conformation of the tetracation in **23** and **24** in which the bipyridinium moiety is again closest to the porphyrin (a "parallel" orientation, Figure 9). As in the hydroquinol-containing catenanes **14** and **16**, this is evidenced by the chemical shift differences between the two β-proton environments being largest, compared to other protons.

A dynamic ^{1}H NMR study of **23** and **24** revealed the existence of a second exchange process in solution in association with the expected rotation of the tetracation macrocycle observed in the hydroquinol catenanes. At high temperatures (105 °C, dimethyl-d_6 sulfoxide), both processes are fast on the NMR time scale, resulting in single resonances for all protons within **23** and **24** (Table 5). Upon cooling to −35 °C (CD_3CN), however, eight bipyridinium peaks and several multiplets ($^+NCH_2$ and $-C_6H_4-$) are observed for the tetracation resonances. At this temperature, the resonances of the methyl and ethyl groups on the porphyrin periphery are split into equal intensity peaks, giving two methyl singlets and two ethyl triplets; however, no change is observed in the methylene resonances.[67] These results may be interpreted as the slowing of the tetracation rotation to differentiate between "inside" and "outside" bipyridinium environments (Figure 9), as observed for **14** and **16**. The extra splitting observed within **23** and **24**, over that observed for the hydroquinol [2]-catenane slow exchange spectra, may be interpreted as the local 2-fold symmetry of the naphthalene ring affecting both the tetracation and the porphyrin subunits of the catenane. At 3 °C, however, the effects of the 2-fold symmetry have been removed from the spectra; this was interpreted in the non-porphyrinic naphthalene [2]-catenane spectra[20] as a process involving the removal of the naphthalene ring from within the tetracation, reorientation of the ring, followed by recomplexation.[68] This "out, turn around, and in again" [20] process was most conveniently followed using the porphyrin methyl resonance coalescence, since temperature changes also effect the tetracation rotation rates, complicating the pattern of resonances

(67) As was observed for the hydroquinol-containing porphyrin catenanes, the permanent presence of the tetracation enhanced the chemical shift difference between the diastereotropic methylene protons of the porphyrin ethyl groups.

(68) It was reasoned in these studies[20] that reorientation of the napthalene ring within the confines of the tetracationic macrocycle was sterically unfavorable and that the removal–reorientation–recomplexation process was necessary to explain the dynamic behavior.

Table 5. Chemical Shift Values (ppm) for Selected Protons for the Naphthalene-Containing [2]-Catenanes **23** and **24** at Several Temperatures[a]

	23		24	
^{1}H	fast rotation, DMSO, 105 °C	slow rotation, CD_3CN, −35 °C	fast rotation, DMSO, 105 °C	slow rotation, CD_3CN, −35 °C
α	7.92	"outside" 8.37	8.00	"outside" 8.36
		8.30		8.30
		"inside" 7.27		"inside" 7.44
		6.64		6.63
β	5.29	"outside" 6.95	5.42	"outside" 6.96
		6.78		6.77
		"inside" 3.62 (hidden)[c]		"inside" 3.77 (hidden)[c]
		2.68		2.69 (hidden)[c]
$-C_6H_4-$	7.72	7.69	7.73	7.71
		7.56		7.58
		7.55		7.56
$^+NCH_2$	5.43	5.52 – 5.33	5.47	5.49
		4.96		4.98
H23	5.70	5.48 (hidden)[b,d]	5.69	5.49 (hidden)[d]
H24	5.09	5.09	5.12	5.11
H25	1.44	1.22[b]	1.46	1.24

[a] Spectra were recorded at 300 MHz using DMSO (δ 2.49 ppm) and CD_2HCN (δ 1.95 ppm) as references. [b] Assigned by comparison with the differences in shifts in the 1,5-DN38C10-containing [2]-catenane.[20,66] [c] Identified by saturation transfer techniques. [d] From COSY-45 results.

observed. This process was found to have k_c = 134 s^{-1} at T_c of 3 °C (Δν 60 Hz) with a $\Delta G_c^{\ddagger}$ of 13.4 kcal mol^{-1}, which at 25 °C is around 400 times per second. The rotation rate of the tetracation was measured using the coalescence method by following the $^+NCH_2$ resonances. In the case of **23**, a Δν of 149 Hz at T_c of 59 °C gave k_c = 331 s^{-1} with $\Delta G_c^{\ddagger}$ = 15.7 kcal mol^{-1}, which converts to around 10 rotations per second at 25 °C. Identical exchange processes were also observed in the metal free catenane **24**, and the results of these are also given in Table 4. The rates for both processes are not significantly different from the zinc derivative.

Compared to the hydroquinol catenane tetracation macrocycle rotation rates observed for **16** and **17**, *viz.* $\Delta G_c^{\ddagger}$ = 14.4 kcal mol^{-1} and 50 rotations per second (25 °C) and $\Delta G_c^{\ddagger}$ = 14.2 kcal mol^{-1} and 80 rotations per second (25 °C), respectively, the naphthalene catenane rotation rates are smaller. This reflects the stronger π–π electron interaction of the naphthalene ring with the tetracation, increasing the free energies of activation and resulting in slower rotation rates.

Within the non-porphyrinic 1,5-DN38C10-based [2]-catenane, the "out, turn around, and in again" process was found to have a $\Delta G_c^{\ddagger}$ of 15.8 kcal mol^{-1} with a rate of around 10 times per second (25 °C), and for tetracation rotation, a $\Delta G_c^{\ddagger}$ of 12.7 kcal mol^{-1} and 1200 rotations per second (25 °C)[20] (Table 4). Thus, in comparison, the porphyrin derivatives **23** and **24** have increased rates of complexation/decomplexation for the naphthalene ring yet have slower tetracation rotation rates. The higher activation energy for macrocycle rotation must reflect the influence (either steric or electronic) of the porphyrin. However, the origin of the lower activation barriers for naphthalene decomplexation in **23** and **24** is not immediately clear but nevertheless is not unreasonable, since the porphyrin catenane is not as conformationally flexible as its nonporphyrinic counterpart and may allow the complexation/decomplexation process to occur with less interference from the adjacent ether chains.

Conclusion

Now that the methodological basis for the synthesis of porphyrin-containing [2]-catenanes is established, the way is clear for the next developmental phase in their study. The in-built functionality of these catenanes in the form of the porphyrinic component will now allow access to means by which the molecule may be addressed by chemical, photochemical, and electrochemical methods. A study of the dynamic behavior of the constituent parts relative to each other under the influence of such chemical stimuli should form the basis for a rational approach to the construction of more elaborate porphyrinic devices which may be designed to function in a predictable and purposeful manner. For example, we can show that simple acid–base chemistry directed at the porphyrin can cause a predictable movement of the mechanically linked and charged components reminiscent of an electrical switch or relay, and this is accompanied by an associated effect on the dynamic behavior of the molecule; an analogous photochemical separation of charge represents a molecular photodiode. We believe that, with further development, these molecules may allow entry into the burgeoning areas of molecular engineering and nanotechnology, which hold great promise for the future of electronic systems that can operate at molecular-scale dimensions.

Experimental Section

General Procedure. All solvents were distilled before use and where necessary dried according to literature procedures.[69] Column chromatography on silica was carried out using Merck Silica Gel 60 (230–400 mesh), and alumina chromatography, using Woelm Acid Alumina (activity grade I). Analytical TLC was carried out on Merck Silica Gel 60 F_{254} precoated aluminum sheets.

NMR spectra were acquired using a 300-MHz Bruker AC 300 spectrometer at 298 K, unless otherwise stated. Chemical shifts (δ) are reported in parts per million relative to internal tetramethylsilane (TMS). ^{13}C spectra were referenced against residual solvent peaks. COSY-45, one-bond C–H correlation, and NOESY two-dimensional NMR experiments employed the standard BRUKER parameters unless stated otherwise. Long-range C–H correlation experiments (FLOCK) were parameterized for J_{CH} of 7 or 10 Hz. NOE difference and saturation transfer experiments utilized standard BRUKER pulse programs, with T_1 values generally optimized for the system under investigation.

Ultraviolet spectra were recorded on either a Hitachi U3200 or a Hewlett Packard 8452A diode array spectrophotometer, in acetonitrile unless otherwise stated. Melting points were determined on a Reichert hot stage using a visual detection method and are uncorrected.

Mass spectra were recorded at the University of Adelaide, and microanalyses were performed at the Microanalytical Unit, Research School of Chemistry, Australian National University.

1,4-Bis[2-(2-hydroxyethoxy)ethoxy]benzene Bis(4-methylbenzenesulfonate)[2] (4). 1,4-Bis[2-(2-hydroxyethoxy)ethoxy]benzene[2] (1.92 g, 6.9 mmol) was dissolved in dry CH_2Cl_2 (30 mL) and added dropwise over 30 min to a solution of toluene-*p*-sulfonyl chloride (3.5 g, 18 mmol) in a mixture of dry CH_2Cl_2/triethylamine (TEA) (1:1) (60 mL) cooled in an ice bath under an N_2 atmosphere, and the resulting solution was stirred at room temperature overnight. The solution was then diluted with H_2O (30 mL) and poured onto crushed ice; the organic layer was isolated, washed with H_2O, 0.05 M HCl solution, and H_2O, and dried (Na_2SO_4). Final purification was carried out using column chromatography (silica)

(69) *Vogel's Textbook of Practical Organic Chemistry*, 4th ed.; Furniss, B. S., Hannaford, A. J., Rogers, V., Smith, P. W. G., Tatchell, A. R., Eds.; Longman: New York, 1978; Chapter 4.

with CH_2Cl_2/MeOH (2%) as the eluant. Concentration of the product fractions gave **4** as an oil, which solidified on standing (2.03 g, 51%): mp 96–7 °C (lit.[2] mp 96–97 °C); ^{1}H NMR ($CDCl_3$) δ 7.80 (4H, d, J = 8 Hz, Ar-H), 7.31 (4H, d, J = 8 Hz, Ar-H), 6.82 (4H, s, Ar-H), 4.21–4.18 (4H, m, α-OCH_2), 4.02–3.98 (4H, m, β-OCH_2), 3.78–3.74 (8H, m, γ-, δ-OCH_2), 2.42 (6H, s, CH_3).

1,4-Bis[2-[2-(*o*-formylphenoxy)ethoxy]ethoxy]benzene (6). Salicylaldehyde (0.92 g, 7.5 mmol) in dry CH_3CN (40 mL) and K_2CO_3 (3.46 g, 25 mmol) were heated under N_2 at 50 °C for 30 min. Ditosylate **4** (2.03 g, 3.4 mmol) dissolved in dry CH_3CN (100 mL) was then added dropwise and the solution refluxed for 30 h. Upon cooling, the solution was filtered and the filtrate taken to dryness by rotary evaporation. The residual solids were partitioned between H_2O and CH_2Cl_2, and the organic layer was isolated, washed (H_2O), and dried (Na_2SO_4). Concentration gave a brown oil (1.7 g, quantitative yield): ^{1}H NMR ($CDCl_3$) δ 10.52 (2H, s, CHO), 7.82 (2H, d, J = 9 Hz, Ar-H), 7.52 (2H, t, J = 9 Hz, Ar-H), 7.05–6.97 (4H, m, Ar-H), 6.83 (4H, s, Ar-H), 4.27 (4H, m, OCH_2), 4.09 (4H, m, OCH_2), 3.97 (4H, m, OCH_2), 3.90 (4H, m, OCH_2); MS m/z 495.2018 (MH^+), $C_{28}H_{31}O_8$ requires 495.20188.

2,8,12,18-Tetraethyl-3,7,13,17-tetramethyl-5,15-{1,4-phenylenebis-[[[[(oxyethylene)oxy]ethylene]oxy]phenyl]}porphyrin (8). The method follows that outlined by Maruyama *et al.*[43,70] for porphyrin synthesis. Dialdehyde **6** (0.39 g, 0.78 mmol) and (3,3′-diethyl-4,4′-dimethyl-2,2′-dipyrryl)methane[42] (0.35 g, 1.53 mmol) were suspended with stirring in dry CH_3CN (75 mL) under an N_2 atmosphere. Trichloroacetic acid (≈35 mg) was added and the solution stirred at room temperature for 5 h. *o*-Chloranil (1.50 g, 4.3 mmol) in dry tetrahydrofuran (THF) (30 mL) was then added and the solution stirred overnight. The solvent was removed by rotary evaporation, the residue was partly taken up in MeOH and filtered, and the filtrate was taken to dryness again. The solids were then dissolved in CH_2Cl_2 and passed through an alumina column using CH_2Cl_2 as the eluant. A final purification was then undertaken using column chromatography (silica) with CH_2Cl_2/Et_2O (3%) as the eluant, and recrystallization (CH_2Cl_2/MeOH) yielded the desired porphyrin **8** (0.11 g, 16%): mp >320 °C; FABMS 913 (M^+) ($C_{58}H_{64}N_4O_6$ requires 913.2); UV (λ_{max}) 406, 504, 538, 572 nm; ^{1}H NMR ($CDCl_3$) δ 10.27 (2H, s, *meso*-H), 7.77 (2H, t, J = 6 Hz, Ar-H), 7.54 (2H, d, J = 6 Hz, Ar-H), 7.35–7.28 (4H, m, Ar-H), 4.34 (4H, m, OCH_2), 4.05 (8H, q, J = 6Hz, CH_2CH_3), 3.47 (4H, m, OCH_2), 3.83 (4H, s, Ar-H), 2.98 (4H, m, OCH_2), 2.61 (12H, s, CH_3), 1.85 (12H, t, J = 6 Hz, CH_3CH_2), 1.75 (4H, m, OCH_2), –2.08 (2H, bs, pyrrole NH); ^{13}C NMR ($CDCl_3$) δ 157.92, 149.85, 145.32, 144.54, 140.86, 135.87, 134.72, 130.92, 130.23, 121.08, 114.09, 112.41, 110.66, 96.25, 69.58, 67.23, 66.22, 63.63, 19.91, 17.69, 13.60. Single crystals suitable for X-ray crystallography were grown from CH_2Cl_2 by infusion of MeOH.

1,1′-[1,4-Phenylenebis(methylene)]bis(4,4′-bipyridinium) Bis(hexafluorophosphate)[58] (12). 1,4-Bis(bromomethyl)benzene (**13**) (1.0 g, 3.7 mmol) was dissolved in CH_3CN/$CHCl_3$ (1:2) (30 mL) and added dropwise over 1 h to a refluxing solution of 4,4′-bipyridine (1.94 g, 12.4 mmol) in CH_3CN (40 mL). The condenser was then reversed and the $CHCl_3$ distilled off, with refluxing continued for 5 h. Upon cooling, the precipitated material was removed by filtration and washed with CH_3CN. The solids were then dissolved in H_2O (with heating), and saturated NH_4PF_6 solution was added until no further precipitation was evident. The white product was removed by filtration, washed with H_2O, and pumped dry (2.50 g, 96%): ^{1}H NMR (acetone-d_6) δ 9.33 (4H, d, J = 7 Hz, α-bipy$^+$), 8.85 (4H, d, J = 7 Hz, α-bipy), 8.66 (4H, d, J = 7 Hz, β-bipy$^+$), 7.96 (4H, d, J = 7 Hz, β-bipy), 7.80 (4H, s, C_6H_4), 6.16 (4H, s, CH_2).

[2,8,12,18-Tetraethyl-3,7,13,17-tetramethyl-5,15-{1,4-phenylenebis-[[[[(oxyethylene)oxy]ethylene]oxy]phenyl]}porphyrinato]zinc(II)·5,12,19,-26-Tetraazoniaheptacyclo[24.2.2.2.$2^{2,5}$.$2^{7,10}$.$2^{12,15}$.$2^{16,19}$.$2^{21,24}$]tetraconta-2,4,7,9,12,14,16,18,21,23,26,28,29,31,33,35,37,39-octadecaene Tetrakis(hexafluorophosphate) (14). Zinc was inserted into the porphyrin **8** using the standard technique ($Zn(OAc)_2$/CH_2Cl_2/MeOH).[71] Zinc porphyrin **9** (111 mg, 1.14×10^{-4} mol), 1,1′-[1,4-phenylenebis(methylene)]-bis(4,4′-bipyridinium) bis(hexafluorophosphate) (**12**) (97 mg, 1.4×10^{-4} mol), 1,4-bis(bromomethyl)benzene (**13**) (45 mg, 1.71×10^{-4} mol), and catalytic amounts of NaI and NH_4PF_6 were combined in dry DMF (5 mL) and stirred at room temperature for 7 days. The solvent was then removed under high vacuum, CH_2Cl_2 was added, and the solid material was removed by filtration. The residual solids were then purified using column chromatography (silica) with MeOH/2 M NH_4Cl solution/$MeNO_2$ (7:2:1) as the eluant. The product fractions were then taken to dryness, partially dissolved in MeOH, filtered, and taken to dryness again. The residue was then dissolved in a minimum amount of H_2O/MeOH (with heating) and filtered cold, and saturated NH_4PF_6 solution was added until precipitation was complete. The product was removed by filtration, washed (H_2O), and pumped dry to yield **14** (47 mg, 20%): FABMS 2075 (M^+), 1929 ($M^+ - PF_6^-$), 1866 ($M^+ - PF_6^- - Zn$), 1785 ($M^+ - 2PF_6^-$), 1721 ($M^+ - 2PF_6^- - Zn$), 1640 ($M^+ - 3PF_6^-$), 1576 ($M^+ - 3PF_6^- - Zn$), 974 (M^+ – tetracation – $4PF_6^-$), 912 (M^+ – tetracation – $4PF_6^-$ – Zn) [$C_{94}H_{94}N_8O_6Zn(PF_6)_4$ requires M^+ 2074.5]; UV (λ_{max}) 422, 544, 578 nm; ^{1}H NMR (105 °C, [$^2H_6$]DMSO) δ 9.73 (2H, s, *meso*-H), 8.06 (8H, bs, α-bipy), 7.90 (2H, t, J = 7 Hz, Ar-H), 7.67 (2H, d, J = 7 Hz, Ar-H), 7.60 (2H, d, J = 7 Hz, Ar-H), 7.46 (8H, s, $-C_6H_4-$), 7.41 (2H, t, J = 7 Hz, Ar-H), 5.87 (8H, bs, β-bipy), 5.28 (8H, s, $^+NCH_2$), 4.58 (4H, m, OCH_2), 4.09 (4H, m, $CHHCH_3$), 3.79 (4H, m, $CHHCH_3$), 3.65 (4H, m, OCH_2), 2.77 (4H, m, OCH_2), 2.88 (4H, m, OCH_2), 2.53 (12H, s, CH_3), 2.44 (4H, s, Ar-H), 1.78 (12H, t, J = 7 Hz, CH_3CH_2); (–13 °C, acetone-d_6) δ 9.92 (2H, s, *meso*-H), 9.03 (4H, d, J = 7 Hz, α-bipy "outside"), 7.91 (6H, m, Ar-H, β-bipy "outside"), 7.54 (6H, m, Ar-H, $-C_6H_4-$), 7.74 (8H, m, 2Ar-H, $-C_6H_4-$), 7.36 (4H, d, J = 7 Hz, α-bipy "inside"), 5.81 (4H, s, $^+NCH_2$), 5.29 (4H, s, $^+NCH_2$), 4.84 (4H, bs, OCH_2), 4.21 (4H, m, $CHHCH_3$), 4.04 (4H, bs, OCH_2), 3.82 (8H, m, $CHHCH_3$, β-bipy "inside"), 3.51 (4H, bs, OCH_2), 3.02 (4H, bs, OCH_2), 2.75 (4H, s, Ar-H), 2.56 (12H, s, CH_3), 1.76 (12H, t, J = 7 Hz, CH_3CH_2). Anal. ($C_{94}H_{94}F_{24}N_8O_6P_4Zn·H_2O$) C, H, N.

General Catenane Demetalation Procedure. Metaled [2]-catenane was stirred in a solution containing 2 M HCl, MeOH, acetone, and NH_4Cl for 5 h. The organic solvents were removed by rotary evaporation, and the solution was filtered and saturated NH_4PF_6 solution added. The precipitated metal free [2]-catenane was removed by filtration, washed with phosphate buffer (pH 6.85) solution, NH_4PF_6 solution, and H_2O, and pumped dry. Product identity was confirmed by UV, ^{1}H NMR spectroscopy, and FAB-MS.

2,8,12,18-Tetraethyl-3,7,13,17-tetramethyl-5,15-{1,4-phenylenebis-[[[[(oxyethylene)oxy]ethylene]oxy]phenyl]}porphyrin·5,12,19,26-Tetraazoniaheptacyclo[24.2.2.2.$2^{2,5}$.$2^{7,10}$.$2^{12,15}$.$2^{16,19}$.$2^{21,24}$]tetraconta-2,4,7,9,-12,14,16,18,21,23,26,28,29,31,33,35,37,39-octadecaene Tetrakis(hexafluorophosphate) (15). The [2]-catenane **14** was demetalated using the general procedure described above to yield **15**: FABMS 2012 (M^+), 1867 ($M^+ - PF_6^-$), 1722 ($M^+ - 2PF_6^-$), 1577 ($M^+ - 3PF_6^-$), 1432 ($M^+ - PF_6^-$) [$C_{94}H_{96}N_8O_6(PF_6)_4$ requires M^+ 2012.6]; UV (λ_{max}) 412, 506, 538, 570 nm; ^{1}H NMR (105 °C, [$^2H_6$]DMSO) δ 9.92 (2H, s, *meso*-H), 8.14 (10H, m, Ar-H, α-bipy), 7.96 (2H, t, J = 7 Hz, Ar-H), 7.72 (4H, d, J = 7 Hz, Ar-H), 7.50 (8H, s, $-C_6H_4-$), 7.48 (2H, t, J = 7 Hz, Ar-H), 5.96 (8H, bs, β-bipy), 5.34 (8H, s, $^+NCH_2$), 4.61 (4H, m, OCH_2), 4.19 (4H, m, $CHHCH_3$), 3.87 (4H, m, $CHHCH_3$), 3.69 (4H, m, OCH_2), 3.39 (4H, m, OCH_2), 2.89 hidden (4H, m, OCH_2), 2.59 (12H, s, CH_3), 2.47 (4H, s, Ar-H), 1.79 (12H, t, J = 7 Hz, CH_3CH_2), –3.55 (2H, s, pyrrole NH); (–40 °C, acetone-d_6) δ 10.17 (2H, s, *meso*-H), 9.03 (4H, d, J = 6 Hz, α-bipy "outside"), 7.96 (2H, t, J = 7 Hz, Ar-H), 7.89 (4H, d, J = 6 Hz, β-bipy "outside"), 7.80 (2H, d, J = 7 Hz, Ar-H), 7.75 (4H, d, J = 7 Hz, $-C_6H_4-$), 7.62 (4H, d, J = 6 Hz, α-bipy "inside"), 7.55 (4H, d, J = 7 Hz, $-C_6H_4-$), 7.52 (2H, d, J = 7 Hz, Ar-H), 7.44 (2H, t, J = 7 Hz, Ar-H), 5.82 (4H, s, $^+NCH_2$), 5.34 (4H, s, $^+NCH_2$), 4.88 (4H, m, OCH_2), 4.36 (8H, m, $CHHCH_3$, β-bipy "inside"), 3.84 (8H, m, $CHHCH_3$, OCH_2), 3.57 (4H, m, OCH_2), 3.00 (4H, m, OCH_2), 2.78 (4H, s, Ar-H), 2.61 (12H, s, CH_3), 1.72 (12H, t, J = 7 Hz, CH_3CH_2), –3.72 (2H, bs, pyrrole NH).

1,4-Bis[2-[2-(2-hydroxyethoxy)ethoxy]ethoxy]benzene bis(4-methylbenzenesulfonate)[34] (5). 1,4-Bis[2-[2-(2-hydroxyethoxy)ethoxy]ethoxy]-benzene (1.02 g, 2.7 mmol) was dissolved in dry CH_2Cl_2 (30 mL) and dry triethylamine (TEA) (30 mL) and cooled in an ice bath under N_2. Toluene-*p*-sulfonyl chloride (1.31 g, 6.9 mmol) in dry CH_2Cl_2 (30 mL) was added dropwise, and the solution was stirred at room temperature overnight. The solution was diluted with H_2O (30 mL) and poured onto crushed ice. The organic layer was isolated, washed (2 M HCl solution and H_2O), and dried (Na_2SO_4). A final purification was carried out on a chromatography column (silica) using CH_2Cl_2/MeOH (2%) as the eluant, producing **5** as a yellow oil (0.94 g, 50%):[34] ^{1}H NMR ($CDCl_3$) δ 7.77 (4H, d, J = 7 Hz, Ar-H), 7.30 (4H, d, J = 7 Hz, Ar-H), 6.81 (4H, s, Ar-H), 4.14 (4H, m, α-OCH_2), 4.03 (4H, m, β-OCH_2), 3.77 (4H, m, γ-OCH_2), 3.69–3.59 (12H, m, OCH_2), 2.41 (6H, s, CH_3).

1,4-Bis[2-[2-[2-(*o*-formylphenoxy)ethoxy]ethoxy]ethoxy]benzene (7). Ditosylate **5** (0.94 g, 1.38 mmol), salicylaldehyde (0.37 g, 3.04 mmol), and K_2CO_3 (0.95 g, 6.9 mmol) were combined in dry CH_3CN (60 mL),

(70) Osuka, A.; Kobayashi, F.; Maruyama, K. *Bull. Chem. Soc. Jpn.* **1991**, *64*, 1213–1225.

(71) Smith, K. M. *Porphyrins and Metalloporphyrins*; Elsevier: Amsterdam, 1975; Chapter 5.

and the solution was refluxed under N_2 for 32 h. Upon cooling, the solution was filtered, and the filtrate was taken to dryness using rotary evaporation. The residue was partitioned between H_2O and CH_2Cl_2, and the organic layer was separated, washed (H_2O), and dried (Na_2SO_4). The product was purified by column chromatography (silica) using CH_2Cl_2/MeOH (3%) as the eluant, to yield **7** as a yellow oil (0.19 g, 24%): ^{1}H NMR ($CDCl_3$) δ 10.48 (2H, s, CHO), 7.78 (2H, d, J = 8 Hz, Ar-H), 7.47 (2H, t, J = 8 Hz, Ar-H), 6.98 (2H, t, J = 8 Hz, Ar-H), 6.92 (2H, d, J = 8 Hz, Ar-H), 6.80 (4H, s, Ar-H), 4.20 (4H, t, J = 4 Hz, OCH_2), 4.02 (4H, t, J = 4 Hz, OCH_2), 3.88 (4H, m, OCH_2), 3.77 (4H, m, OCH_2), 3.70 (8H, m, OCH_2); FAB-MS 584 (M + H$^+$) ($C_{32}H_{38}O_{10}$ requires M + H$^+$ 583.6).

2,8,12,18-Tetraethyl-3,7,13,17-tetramethyl-5,15-{1,4-phenylenebis-[[[[[[(oxyethylene)oxy]ethylene]oxy]ethylene]oxy]phenyl]}porphyrin (10). Dialdehyde **7** (0.23 g, 0.39 mmol), (3,3′-diethyl-4,4′-dimethyl-2,2′-dipyrryl)methane[42] (0.18 g, 0.78 mmol), and a catalytic amount of CCl_3CO_2H were dissolved in dry CH_3CN (36 mL), and the solution was stirred at room temperature under N_2 for 5 h. o-Chloranil (0.53 g, 2.2 mmol) dissolved in dry THF (24 mL) was added all at once, and the solution was stirred overnight. The solvent was removed by rotary evaporation, and the residue was dissolved in CH_2Cl_2 and passed through an alumina column using CH_2Cl_2 as the eluant. A final purification was carried out using a silica column employing CH_2Cl_2/Et_2O (10%) followed by CH_2Cl_2/Et_2O (4:1) + EtOH (2%) as eluants to yield the porphyrin **10** (60 mg, 15%): FAB-MS 1000 (M$^+$) ($C_{62}H_{72}N_4O_8$ requires M$^+$ 1000.5); UV (λ_{max}) 406, 504, 538, 574 nm; ^{1}H NMR ($CDCl_3$) δ 10.22 (2H, s, *meso*-H), 7.71 (2H, t, J = 8 Hz, Ar-H), 7.59 (2H, d, J = 8 Hz, Ar-H), 7.38 (2H, d, J = 8 Hz, Ar-H), 7.32 (2H, t, J = 8 Hz, Ar-H), 5.48 (4H, s, Ar-H), 4.20 (4H, t, J = 4 Hz, OCH_2), 4.04 (8H, m, CH_2CH_3), 3.35 (4H, t, J = 4 Hz, OCH_2), 2.77 (4H, m, OCH_2), 2.60 (12H, s, CH_3), 2.57 (4H, m, OCH_2), 2.48 (8H, s, OCH_2), 1.81 (12H, t, J = 6 Hz, CH_3CH_2), -2.26 (2H, bs, pyrrole NH); ^{13}C NMR ($CDCl_3$) δ 158.35, 151.70, 145.40, 144.20, 140.84, 135.83, 134.89, 130.09, 121.02, 114.82, 111.93, 96.03, 69.99, 69.79, 68.85, 68.60, 68.49, 66.50, 19.94, 17.70, 13.57. Single crystals suitable for X-ray crystallography were grown from CH_2Cl_2 by infusion of MeOH.

[2,8,12,18-Tetraethyl-3,7,13,17-tetramethyl-5,15-{1,4-phenylenebis-[[[[[[(oxyethylene)oxy]ethylene]oxy]ethylene]oxy]phenyl]}porphyrinato]-zinc(II)·5,12,19,26-Tetraazoniaheptacyclo[24.2.2.2.2^{2,5}.2^{7,10}.2^{12,15}.2^{16,19}.2^{21,24}]-tetraconta-2,4,7,9,12,14,16,18,21,23,26,28,29,31,33,35,37,39-octadecaene Tetrakis(hexafluorophosphate) (16). Zinc was inserted into **10** using a well-developed technique ($Zn(OAc)_2/CH_2Cl_2$/MeOH)[71] to give **11** (FAB-MS 1062 (M$^+$)). **11** (50 mg, 4.7 × 10^{-5} mol), 1,1′-[1,4-phenylenebis(methylene)]bis(4,4′-bipyridinium)bis(hexafluorophosphate) (**12**) (40 mg, 5.6 × 10^{-5} mol), 1,4-bis(bromomethyl)benzene (**13**) (18.6 mg, 7.0 × 10^{-5} mol), and catalytic amounts of NaI and NH_4PF_6 were stirred at room temperature for 14 days in a minimum volume of dry DMF (~3 mL). The solvent was removed under high vacuum, and the remaining solids were washed well with CH_2Cl_2. The residual material was purified using column chromatography employing MeOH/2 M NH_4Cl solution/$MeNO_2$ (7:2:1) as the eluant. The product fractions were taken to dryness, dissolved in a minimum amount of MeOH, filtered, and taken to dryness again. The solids were then dissolved in a minimum volume of H_2O/MeOH (with heating) and filtered cold, and saturated NH_4PF_6 solution was added. The precipitated catenane **16** was collected by filtration, washed with H_2O, and pumped dry (28 mg, 28%): FAB-MS 2162 (M$^+$), 2018 (M$^+$ - PF_6^-), 1955 (M$^+$ - PF_6^- - Zn), 1873 (M$^+$ - 2PF_6^-), 1809 (M$^+$ - 2PF_6^- - Zn), 1728 (M$^+$ - 3PF_6^-), 1664 (M$^+$ - 3PF_6^- - Zn), 1583 (M$^+$ - 4PF_6^-) [$C_{98}H_{102}N_8O_8Zn(PF_6)_4$ requires M$^+$ 2162.5]; UV (λ_{max}) 422, 544, 578 nm; ^{1}H NMR (70 °C, CD_3CN) δ 9.78 (2H, s, *meso*-H), 7.94 (2H, t, J = 7 Hz, Ar-H), 7.80 (8H, d, J = 7 Hz, α-bipy), 7.66 (2H, d, J = 7 Hz, Ar-H), 7.63 (2H, d, J = 7 Hz, Ar-H), 7.45 (2H, t, J = 7 Hz, Ar-H), 7.37 (8H, s, $-C_6H_4-$), 5.76 (8H, d, J = 8 Hz, β-bipy), 5.26 (8H, s, $^+NCH_2$), 4.56 (4H, m, OCH_2), 4.17 (4H, m, $CHHCH_3$), 3.83 (4H, m, $CHHCH_3$), 3.58–3.44 (16H, m, OCH_2), 2.96 (4H, m, OCH_2), 2.63 (12H, s, CH_3), 2.59 (4H, s, Ar-H), 1.83 (12H, t, J = 7 Hz, CH_3CH_2); ^{1}H NMR (-40 °C, acetone-d_6) δ 9.71 (2H, s, *meso*-H), 8.99 (4H, bs, α-bipy "outside"), 7.95 (2H, t, J = 7 Hz, Ar-H), 7.86 (4H, bs, β-bipy "outside"), 7.80–7.68 (8H, m, 2Ar-H, $-C_6H_4-$), 7.62 (4H, bs, α-bipy "inside"), 7.52 (6H, m, Ar-H, $-C_6H_4-$), 5.82 (4H, bs, $^+NCH_2$), 5.67 (4H, bs, $^+NCH_2$), 4.48 (4H, m, OCH_2), 4.43 (4H, m, $CHHCH_3$), 3.76 (4H, m, $CHHCH_3$), 3.74 hidden (4H, β-bipy "inside"), 3.71–3.38 (16H, m, OCH_2), 3.08 (4H, m, OCH_2), 2.59 (12H, s, CH_3), 1.78 (12H, t, J = 7 Hz, CH_3CH_2). Anal. ($C_{98}H_{102}F_{24}N_8O_8P_4Zn$) C, H, N.

2,8,12,18-Tetraethyl-3,7,13,17-tetramethyl-5,15-{1,4-phenylenebis-[[[[[(oxyethylene)oxy]ethylene]oxy]ethylene]oxy]phenyl]}porphyrin·5,12,-19,26-Tetraazoniaheptacyclo[24.2.2.2.2^{2,5}.2^{7,10}.2^{12,15}.2^{16,19}.2^{21,24}]tetraconta-2,4,7,9,12,14,16,18,21,23,26,28,29,31,33,35,37,39-octadecaene Tetrakis(hexafluorophosphate) (17). The zinc contained within the porphyrin moiety of the [2]-catenane **16** was removed using the general procedure described above to yield the metal free catenane **17**. FAB-MS 2100 (M$^+$), 1956 (M$^+$ - PF_6^-), 1811 (M$^+$ - 2PF_6^-), 1666 (M$^+$ - 3PF_6^-), 1520 (M$^+$ - 4PF_6^-) [$C_{98}H_{104}N_8O_8(PF_6)_4$ requires M$^+$ 2100.6] UV (λ_{max}) 412, 504, 536, 572 nm; ^{1}H NMR (70 °C, CD_3CN) δ 9.95 (2H, s, *meso*-H), 7.97 (2H, t, J = 7 Hz, Ar-H), 7.83 (8H, d, J = 7 Hz, α-bipy), 7.74 (2H, d, J = 7 Hz, Ar-H), 7.69 (2H, d, J = 7 Hz, Ar-H), 7.49 (2H, t, J = 7 Hz, Ar-H), 7.39 (8H, s, $-C_6H_4-$), 5.82 (8H, d, J = 7 Hz, β-bipy), 5.27 (8H, s, $^+NCH_2$), 4.52 (4H, m, OCH_2), 4.23 (4H, m, $CHHCH_3$), 3.87 (4H, m, $CHHCH_3$), 3.58 (8H, m, OCH_2), 3.46 (8H, m, OCH_2), 2.98 (4H, m, OCH_2), 2.66 (12H, s, CH_3), 2.62 (4H, s, Ar-H), 1.80 (12H, t, J = 7 Hz, CH_3CH_2), -3.46 (2H, bs, pyrrole NH); ^{1}H NMR (-35 °C, CD_3CN) δ 9.79 (2H, s, *meso*-H), 8.48 (4H, bs, α-bipy "outside"), 7.97 (4H, m, 2Ar-H), 7.66 (2H, d, J = 7 Hz, Ar-H), 7.52 (2H, t, J = 7 Hz, Ar-H), 7.42 (8H, β-bipy "outside", $-C_6H_4-$), 7.32 (4H, bs, $-C_6H_4-$), 7.15 (4H, bs, α-bipy "inside"), 5.41 (4H, bs, $^+NCH_2$), 5.22 (4H, bs, $^+NCH_2$), 4.39 (4H, bs, OCH_2), 4.35 (4H, m, $CHHCH_3$), 3.79 (4H, m, $CHHCH_3$), 3.53 (8H, m, OCH_2, β-bipy "inside" hidden), 3.47 (4H, m, OCH_2), 3.33 (4H, m, OCH_2), 3.17 (4H, m, OCH_2), 2.85 (4H, m, OCH_2), 2.63 (12H, s, CH_3), 1.74 (12H, t, J = 7 Hz, CH_3CH_2), -3.89 (2H, bs, pyrrole NH).

1,5-Bis[2-[2-(2-hydroxyethoxy)ethoxy]ethoxy]naphthalene (18). 1,5-Dihydroxynaphthalene (10.58 g, 66 mmol) and K_2CO_3 (36.52 g, 264 mmol) were combined in dry CH_3CN (180 mL) and stirred mechanically with heating under N_2 for 10 min. 2-(2′-(2″-Chloroethoxy)ethoxy)-ethanol (24.50 g, 145 mmol) dissolved in CH_3CN (100 mL) was added dropwise, and the resulting solution was refluxed under N_2 for 7 days. Upon cooling, the solution was filtered and taken to dryness by rotary evaporation. The residue was partitioned between CH_2Cl_2 and H_2O, and the organic layer was separated, washed (H_2O, 1 M HCl solution, and H_2O), and dried (Na_2SO_4). Final purification was carried out using column chromatography (silica) with CH_2Cl_2/MeOH (5%) as the eluant to yield **18** as a golden brown oil that solidified upon standing (25.2 g, 89%): mp 67–8 °C; FAB-MS 424.2 (M$^+$) ($C_{22}H_{32}O_8$ requires M$^+$ 424.21); ^{1}H NMR ($CDCl_3$) δ 7.85 (2H, d, J = 9 Hz, Ar-H), 7.34 (2H, t, J = 9 Hz, Ar-H), 6.81 (2H, d, J = 9 Hz, Ar-H), 4.26 (4H, t, J = 4 Hz, α-OCH_2), 3.96 (4H, t, J = 4 Hz, β-OCH_2), 3.76 (4H, m, OCH_2), 3.67 (8H, m, OCH_2), 3.57 (4H, m, OCH_2). Anal. ($C_{22}H_{32}O_8$) C, H.

1,5-Bis[2-[2-(2-hydroxyethoxy)ethoxy]ethoxy]naphthalene Bis(4-methylbenzenesulphonate) (19). 1,5-Bis[2-[2-(2-hydroxyethoxy)ethoxy]-ethoxy]naphthalene **18** (4.14 g, 9.8 mmol) was dissolved in dry CH_2Cl_2/TEA (1:1) and cooled in an ice bath under N_2. Toluene-p-sulfonyl chloride (4.65 g, 24 mol) in dry CH_2Cl_2/TEA (1:1) was added dropwise and the resulting solution stirred at room temperature overnight. The solution was then poured onto crushed ice and diluted with H_2O. The organic layer was separated, washed (1 M HCl solution and H_2O), and dried (Na_2SO_4). Purification was carried out by column chromatography (silica) using CH_2Cl_2/MeOH (2%) as the eluant to yield **19** as a light yellow oil (4.23 g, 59%): ^{1}H NMR ($CDCl_3$) δ 7.85 (4H, d, J = 9 Hz, Ar-H), 7.78 (2H, d, J = 9 Hz, Ar-H), 7.36 (4H, d, J = 9 Hz, Ar-H), 7.31 (2H, t, J = 9 Hz, Ar-H), 6.84 (2H, d, J = 9 Hz, Ar-H), 4.28 (4H, t, J = 4 Hz, OCH_2), 4.15 (4H, t, J = 4 Hz, OCH_2), 3.96 (4H, t, J = 4 Hz, OCH_2), 3.76–3.64 (8H, m, OCH_2), 3.62 (4H, m, OCH_2), 2.40 (6H, s, CH_3).

1,5-Bis[2-[2-[2-(o-formylphenoxy)ethoxy]ethoxy]ethoxy]naphthalene (20). Salicylaldehyde (1.55 g, 13 mmol) and K_2CO_3 (3.18 g, 23 mmol) were stirred with heating in dry CH_3CN (40 mL) under N_2. Naphthalene ditosylate derivative **19** (4.23 g, 5.77 mmol) in dry CH_3CN was added all at once and the solution refluxed for 50 h. Upon cooling, the solvent was removed by rotary evaporation, and the residue was partitioned between H_2O and CH_2Cl_2. The organic layer was isolated, washed (H_2O), and dried (Na_2SO_4). The product was purified using column chromatography (silica) with CH_2Cl_2/MeOH (2%) as the eluant to give **20** as a dark yellow oil (2.88 g, 79%): MS m/z 632.2621 (M$^+$) $C_{36}H_{40}O_{10}$ requires M$^+$ 632.26213; ^{1}H NMR ($CDCl_3$) δ 10.51 (2H, s, CHO), 7.84 (4H, t, J = 9 Hz, Ar-H), 7.50 (2H, t, J = 6 Hz, Ar-H), 7.32 (2H, t, J = 8 Hz, Ar-H), 7.01 (2H, t, J = 8 Hz, Ar-H), 6.93 (2H, d, J = 8 Hz, Ar-H), 6.82 (2H, d, J = 8 Hz, Ar-H), 4.29 (4H, t, J = 4 Hz, OCH_2), 4.21 (4H, t, J = 4 Hz, OCH_2), 3.99 (4H, t, J = 4Hz, OCH_2), 3.92 (4H, t, J = 4 Hz, OCH_2), 3.84–3.76 (8H, m, OCH_2). Anal. ($C_{36}H_{40}O_{10}$) C, H.

2,8,12,18-Tetraethyl-3,7,13,17-tetramethyl-5,15-{1,5-naphthylenebis-[[[[[(oxyethylene)oxy]ethylene]oxy]ethylene]oxy]phenyl]}porphyrin (21). Dialdehyde **20** (0.88 g, 1.4 mmol) was combined with (3,3′-diethyl-4,4′-dimethyl-2,2′-dipyrryl)methane[42] (0.62 g, 2.7 mmol) and a catalytic amount of CCl_3CO_2H in dry CH_3CN (135 mL) under an N_2 blanket and stirred at room temperature for around 5 h. *o*-Chloranil (1.86 g, 7.6 mmol) in dry THF was added all at once and the solution stirred overnight. The solution was then taken to dryness, and the residue was passed through an alumina column using CH_2Cl_2 and CH_2Cl_2/MeOH (10%) as eluants. A final purification was carried out using a combination of column chromatography (silica) and fractional crystallization with CH_2Cl_2/MeOH, yielding **21** (127 mg, 9%): FAB-MS 1051 (M^+) ($C_{66}H_{74}N_4O_8$ requires 1050.5); ^1H NMR ($CDCl_3$) δ 10.22 (2H, s, *meso*-H), 7.77 (2H, t, J = 6 Hz, Ar-H), 7.54 (2H, d, J = 6Hz, Ar-H), 7.39 (2H, d, J = 8 Hz, Ar-H), 7.31 (2H, t, J = 8 Hz, Ar-H), 7.17 (2H, d, J = 8 Hz, Ar-H), 6.32 (2H, t, J = 8 Hz, Ar-H), 5.03 (2H, d, J = 8 Hz, Ar-H), 4.22 (4H, t, J = 5 Hz, OCH_2), 4.04 (8H, q, J = 7 Hz, CH_2CH_3), 3.33 (4H, t, J = 5 Hz, OCH_2), 2.84 (4H, t, J = 4 Hz, OCH_2), 2.67–2.62 (24H, m, OCH_2), 1.81 (12H, t, J = 7 Hz, CH_3CH_2), –2.26 (2H, bs, pyrrole NH); ^{13}C NMR ($CDCl_3$) δ 158.24, 152.99, 145.43, 144.23, 140.83, 135.81, 135.00, 131.22, 130.08, 126.08, 124.22, 121.02, 114.10, 113.74, 111.79, 105.35, 96.04, 69.89, 69.59, 68.66, 68.31, 68.18, 66.36, 19.91, 17.70, 13.53. Anal. ($C_{66}H_{74}N_4O_8$) C, H, N.

[2,8,12,18-Tetraethyl-3,7,13,17-tetramethyl-5,15-{1,5-naphthylenebis-[[[[[(oxyethylene)oxy]ethylene]oxy]ethylene]oxy]phenyl]}porphyrinato]-zinc(II)·5,12,19,26-Tetraazoniaheptacyclo[24.2.2.2^{2,5}.2^{7,10}.2^{12,15}.2^{16,19}.2^{21,24}]-tetraconta-2,4,7,9,12,14,16,18,21,23,26,28,29,31,33,35,37,39-octadecaene Tetrakis(hexafluorophosphate) (23). Zinc was inserted into the naphthalene porphyrin **21** using the standard method ($Zn(OAc)_2$/CH_2Cl_2/MeOH)[71] to produce **22** (UV λ_{max} 414, 542, 576 nm). Zinc naphthalene porphyrin **22** (97 mg, 8.7×10^{-5} mol), 1,1′-[1,4-phenylenebis(methylene)]bis(4,4′-bipyridinium)bis(hexafluorophosphate) (**12**) (61 mg, 8.7×10^{-5} mol), 1,4-bis(bromomethyl)benzene (**13**) (27 mg, 1.04×10^{-4} mol), and catalytic amounts of NaI and NH_4PF_6 were stirred at room temperature in DMF (2 mL) for 11 days. The solvent was then removed under vacuum, and the residue was washed with CH_2Cl_2. Residual solids were then purified using column chromatography (silica) with MeOH/2 M NH_4Cl solution/$MeNO_2$ (7:2:1 v/v) as the eluant. The product fractions were then taken to dryness, partially dissolved in a minimum amount of MeOH, filtered, and taken to dryness again. The remaining solids were then dissolved in a minimum amount of H_2O/MeOH (with heating) and filtered cold, and saturated NH_4PF_6 solution was added until no further precipitation was evident. The catenane **23** was removed by filtration, washed (H_2O), and pumped dry (86 mg, 45%): FAB-MS 2068 ($M^+ - PF_6^-$), 1923 ($M^+ - 2PF_6^-$), 1859 ($M^+ - PF_6^- - Zn$), 1778 ($M^+ - 3PF_6^-$), 1113 (M^+ – tetracation – $4PF_6^-$), 1051 (M^+ – tetracation – $4PF_6^-$ – Zn) [$C_{102}H_{104}N_8O_8Zn(PF_6)_4$ requires $M^+ - PF_6$ 2067.6]; UV (λ_{max}) 422, 544, 578 nm; ^1H NMR ([$^2H_6$]DMSO, 105 °C) δ 9.58 (2H, s, *meso*-H), 7.92 (10H, m, α-bipy, Ar-H), 7.72 (8H, s, $-C_6H_4-$), 7.66 (2H, d, J = 8 Hz, Ar-H), 7.54 (2H, d, J = 7 Hz, Ar-H), 7.39 (2H, t, J = 7 Hz, Ar-H), 5.70 (2H, d, J = 7 Hz, Ar-H), 5.43 (8H, s, $^+NCH_2$), 5.29 (8H, m, β-bipy), 5.09 (2H, t, J = 7 Hz, Ar-H), 4.50 (4H, m, OCH_2), 4.14 (4H, m, $CHHCH_3$), 3.92 (4H, m, OCH_2), 3.74 (8H, m, OCH_2, $CHHCH_3$), 3.62 (4H, m, OCH_2), 3.50 (8H, m, OCH_2), 2.52 (12H, s, CH_3), 1.77 (12H, t, J = 7 Hz, CH_3CH_2), 1.44 (2H, d, J = 7 Hz, Ar-H); ^1H NMR (CD_3CN, –35 °C) δ 9.60 (2H, s, *meso*-H); δ 8.37 (2H, d, J = 6 Hz, α-bipy "outside"), 8.30 (2H, d, J = 6 Hz, α'-bipy "outside"), 7.93 (2H, t, J = 7 Hz, Ar–H), 7.79 (2H, d, J = 7 Hz, Ar-H), 7.69 (2H, d, J = 8 Hz, $-C_6H_4-$), 7.64 (2H, d, J = 7 Hz, Ar-H), 7.56 (4H, s, $-C_6H_4-$), 7.55 (2H, d, J = 8 Hz, $-C_6H_4-$), 7.46 (2H, t, J = 7 Hz, Ar-H), 7.27 (2H, d, J = 6 Hz, α-bipy "inside"), 6.95 (2H, d, J = 6 Hz, β'-bipy "outside"), 6.78 (2H, d, J = 6 Hz, β-bipy "outside"), 6.64 (2H, d, J = 6 Hz, α'-"inside"), 5.52–5.33 (8H, m, $^+NCH_2$ (6H), Ar-H (2H)), 5.09 (2H, t, J = 8 Hz, Ar-H), 4.96 (2H, d, J = 13 Hz, $^+NCH_2$), 4.66 (2H, m, OCH_2), 4.31 (4H, m, $CHHCH_3$), 3.96 (4H, m, OCH_2), 3.62–3.49 (20H, m, β-bipy "inside" (2H), $CHHCH_3$ (4H), OCH_2 (14H)), 3.36 (2H, m, OCH_2), 3.23 (2H, m, OCH_2), 2.68 (2H, d, J = 6Hz, β'-bipy "inside"), 2.64 (6H, s, CH_3), 2.43 (6H, s, CH_3), 1.77 (6H, t, J = 6Hz, CH_3CH_2), 1.67 (6H, t, J = 6 Hz, CH_3CH_2), 1.23 (2H, d, J = 8 Hz, Ar-H). Anal. ($C_{102}H_{104}F_{24}N_8O_8P_4Zn$) C, H, N.

2,8,12,18-Tetraethyl-3,7,13,17-tetramethyl-5,15-{1,5-naphthylenebis-[[[[[(oxyethylene)oxy]ethylene]oxy]ethylene]oxy]phenyl]}porphyrin·5,12,-19,26-Tetraazoniaheptacyclo[24.2.2.2^{2,5}.2^{7,10}.2^{12,15}.2^{16,19}.2^{21,24}]tetraconta-2,4,7,9,12,14,16,18,21,23,26,28,29,31,33,35,37,39-octadecaene Tetrakis(hexafluorophosphate) (24). The metal free derivative **24**, was obtained using the general demetalation procedure described previously. FAB-MS 2006 ($M^+ - PF_6^-$), 1861 ($M^+ - 2PF_6^-$), 1716 ($M^+ - 3PF_6^-$), 1571 ($M^+ - 4PF_6^-$), 1051 (M^+ – tetracation – $4PF_6^-$) [$C_{102}H_{106}N_8O_8(PF_6)_4$ requires $M^+ - PF_6$ 2005.7]; ^1H NMR ([$^2H_6$]DMSO, 105 °C) δ 9.78 (2H, s, *meso*-H), 8.00 (8H, d, J = 6 Hz, α-bipy), 7.95 (2H, t, J = 7 Hz, Ar-H), 7.71 (12H, m, $-C_6H_4-$ (8H), Ar-H (4H)), 7.45 (2H, t, J = 7 Hz, Ar-H), 5.69 (2H, d, J = 8 Hz, Ar-H), 5.47 (8H, s, $^+NCH_2$), 5.42 (8H, d, J = 6 Hz, β-bipy), 5.12 (2H, t, J = 8 Hz, Ar-H), 4.48 (4H, m, OCH_2), 4.17 (4H, m, $CHHCH_3$), 3.94 (4H, m, OCH_2), 3.79 (8H, m, OCH_2 (4H), $CHHCH_3$ (4H)), 3.49 (12H, m, OCH_2), 2.59 (12H, s, CH_3), 1.79 (12H, t, J = 7 Hz, CH_3CH_2), 1.47 (2H, d, J = 8 Hz, Ar-H), –3.58 (2H, bs, pyrrole NH); ^1H NMR (CD_3CN, –35 °C) δ 9.75 (2H, s, *meso*-H), 8.36 (2H, d, J = 6 Hz, α-bipy "outside"), 8.30 (2H, d, J = 6 Hz, α'-bipy "outside"), 7.95 (2H, t, J = 7 Hz, Ar-H), 7.90 (2H, d, J = 7 Hz, Ar-H), 7.71 (2H, d, J = 8 Hz, $-C_6H_4-$), 7.65 (2H, d, J = 7 Hz, Ar-H), 7.58 (4H, s, $-C_6H_4-$), 7.56 (2H, d, J = 8 Hz, $-C_6H_4-$), 7.49 (2H, t, J = 7 Hz, Ar-H), 7.44 (2H, d, J = 6 Hz, α-bipy "inside"), 6.96 (2H, d, J = 6 Hz, β'-bipy "outside"), 6.77 (2H, d, J = 6 Hz, β-bipy "outside"), 6.63 (2H, d, J = 6 Hz, α'-bipy "inside"), 5.58–5.35 (8H, m, Ar-H (2H), $^+NCH_2$ (6H)), 5.11 (2H, t, J = 8 Hz, Ar-H), 4.98 (2H, m, $^+NCH_2$), 4.66 (2H, m, OCH_2), 4.32 (4H, m, $CHHCH_3$), 4.02–3.50 (24H, m, β-bipy "inside" (2H), $CHHCH_3$ (4H), OCH_2 (18H)), 3.26 (4H, m, OCH_2), 2.69 (10H, bs, CH_3 (8H), β'-bipy "inside"), 2.48 (8H, s, CH_3), 1.73 (6H, t, J = 7 Hz, CH_3CH_2), 1.62 (6H, t, J = 7 Hz, CH_3CH_2), 1.24 (2H, d, J = 8 Hz, Ar-H), –4.06 (2H, bs, pyrrole NH).

Acknowledgment. The authors are grateful to the Australian Research Council for financial assistance for part of this work. We also thank Professor J. Fraser Stoddart, Drs. Douglas Philp and Richard Bissell for their advice on catenane synthesis, and Dr. David Tucker for assistance with NMR measurements.

Supplementary Material Available: Figures showing atom numbering schemes and tables listing non-hydrogen positional and isotropic displacement parameters and bond lengths and angles for **8** and **10** (24 pages); structure factor amplitudes for **8** and **10** (45 pages). This material is contained in many libraries on microfiche, immediately follows this article in the microfilm version of the journal, and can be ordered from the ACS; see any current masthead page for ordering information.